Title: Brain Angiopathy and Impaired Glucose Metabolism in Model Mice with Psychiatric-Related Phenotypes

Short title: Angiopathy in model mice and patients with psychosis

Authors: Shinobu Hirai[1,*], Hideki Miwa[1,2], Tomoko Tanaka[1], Kazuya Toriumi[3], Yasuto Kunii[4], Mizuki Hino[4], Ryuta Izumi[4], Atsuko Nagaoka[4], Hirooki Yabe[4], Tomoya Nakamachi[5], Seiji Shioda[6], Takashi Dan[7], Toshio Miyata[7], Yasumasa Nishito[8,] Kazuhiro Suzuki[3], Mitsuhiro Miyashita[3], Masanari Itokawa[3], Makoto Arai[3], Haruo Okado[1,*]

Affiliations: 1, Neural Development Project, Department of Brain Development and Neural Regeneration, Tokyo Metropolitan Institute of Medical Science, Tokyo 156-8506, Japan.

2, Molecular Neuropsychopharmacology Section, Department of Neuropsychopharmacology, National Institute of Mental Health, National Center of Neurology and Psychiatry, Tokyo 187-8553, Japan.

3, Schizophrenia Research Project, Department of Psychiatry and Behavioral Sciences, Tokyo Metropolitan Institute of Medical Science, Tokyo 156-8506, Japan.

4, Department of Neuropsychiatry, School of Medicine, Fukushima Medical University, Fukushima 960-1295, Japan.

5, Laboratory of Regulatory Biology, Graduate School of Science and, Engineering, University of Toyama, Toyama 930-8555, Japan.

6, Global Research Center for Innovative Life Science, Peptide Drug Innovation, Hoshi University, Tokyo 142-8501, Japan.

7, Division of Molecular Medicine and Therapy, Tohoku University Graduate School of Medicine, Miyagi 980-8575, Japan.

8, Center for Basic Technology Research, Tokyo Metropolitan Institute of Medical Science, Tokyo 156-8506, Japan.

*These authors contributed equally to this work.

Correspondence should be addressed to Shinobu Hirai and Haruo Okado, Neural Development Project, Department of Brain Development and Neural Regeneration, Tokyo Metropolitan Institute of Medical Science, Tokyo 156-8506, Japan. E-mail: hirai-sn@igakuken.or.jp (S.H.) and okado-hr@igakuken.or.jp (H.O.)

Abstract: Psychiatric disorders are associated with metabolic dysfunction, but it is unclear whether our current high-sugar diet contributes to pathogenesis. We demonstrate that a high-sucrose diet during adolescence induces behavioral phenotypes of psychiatric disease, such as hyperactivity, poor working memory, anxiety, and impaired sensory gating, in mice deficient for glyoxalase-1, an enzyme involved in detoxification of sucrose metabolites. The high-sucrose diet also induced advanced glycation end product accumulation in brain microcapillary endothelium, disrupted interneuron function and striatal dopamine release, and reduced brain glucose uptake. Aspirin protected against this angiopathy, enhanced brain glucose uptake, and prevented abnormal behavioral phenotypes. Brains from schizophrenia and bipolar disorder patients exhibited similar angiopathy. Psychiatric disorders are associated with microvascular brain damage, possibly due to variety of environmental stresses including metabolic stress.

One Sentence Summary: We demonstrate neural angiopathy and multiple endophenotypes of psychiatric disease in a mouse model of impaired glucose metabolism due to excessive sugar

intake and confirm neural angiopathy in postmortem brains of schizophrenia and bipolar disorder patients.

Main Text: In response to the global increase in dietary sugar intake, the World Health Organization recently published guidelines that addressed concerns about body weight gain and the development of dental caries(*1*). Body weight gain or high-sugar intake alone increases the risks of numerous chronic diseases, including diabetes, hypertension, and kidney disease. However, there are few studies on the effects of high-sugar intake during adolescence on current and future mental health. Teenagers derive higher daily calorie intake from sugar than any other age group (~20% of total daily caloric intake)(*2*). Furthermore, most chronic psychiatric disorders such as schizophrenia (SZ) and bipolar disorder (BD) develop before 30 years of age(*3*, *4*) through complex interactions between multiple genetic and environmental risk factors(*5*). Therefore, excessive sugar intake may contribute to the pathogenesis of psychiatric disorders during this critical prodromal period.

Dietary sugars produce advanced glycation end products (AGEs) through non-enzymatic reactions between the native molecules or intermediate metabolites (reactive carbonyl compounds) and the

amino groups of large biomolecules, including proteins, nucleic acids, and lipids. In addition to disrupting biomolecule function, these AGEs may induce inflammatory reactions through the receptor of AGE (RAGE). Furthermore, these reactions are self-sustaining; for example(*6*), AGEs and reactive carbonyl compounds can produce free radicals and reactive oxygen species (ROS)(*7, 8*) that induce oxidative stress and facilitate additional AGE formation(*9*). Because of this positive feedback relationship, oxidative stress is also called "carbonyl stress"(*10*). There is a large body of evidence for elevated oxidative stress as measured by ROS accumulation and lower reduced glutathione (GSH) levels in patients with psychiatric disorders(*11-15*). This oxidative stress may arise in part from dysregulation of specific detoxification pathways. Glyoxalase I (GLO1), an antioxidant zinc metalloenzyme that protects cells from AGE toxicity by catalyzing the binding of the reactive carbonyl compound methylglyoxal to GSH to form S-lactoyl-glutathione(*16, 17*), is expressed at lower levels in depressive-state BD and major depressive disorder (MDD) patients compared with controls(*18*). Moreover, an SZ patient exhibiting poor convalescence was shown to harbor a frameshift mutation in *GLO1* leading to reduced enzyme activity(*19, 20*).

On the basis of these associations, we hypothesized that excessive sugar intake may contribute to the pathogenesis of psychiatric disorders among genetically susceptible individuals.

We addressed this hypothesis by generating a mouse model on the basis of the gene × environment interaction (G × E) approach and identified angiopathy arising from AGE accumulation in neurovascular endothelial cells as a novel psychiatric disorder phenotype in both a mouse model of high glucose intake and deficient GKO1 activity as well as in brain samples from BD and SZ patients. Furthermore, the mouse model also demonstrated multiple behavioral and neurological phenotypes of psychiatric disease that could be ameliorated by antipsychotic or anti-inflammatory drug treatment.

Results

Behavioral phenotypes of psychiatric disease in mice on a high-sucrose diet

To test our hypothesis that excessive sugar intake during adolescence is an environmental risk factor for psychiatric-related phenotypes, we examined mice fed one of two diets containing the same total calories and caloric proportions of carbohydrates, fat, and proteins (Fig. 1a) but with either starch or sucrose as the main carbohydrate. We investigated four groups of mice fed these diets for 50 days immediately after weaning (from postnatal day 21 to 71, corresponding to the juvenile/adolescent stage): wild-type (WT) starch-fed mice (control, CTL), WT sucrose-fed mice

(environmental stressor, Env), *Glo1* heterozygous knockout starch-fed mice (genetic factor, Gen), and *Glo1* heterozygous knockout sucrose-fed mice (G × E) (Fig. 1a). Western blot analysis revealed that *Glo1* heterozygous mice exhibited reduced GLO1 expression in the cerebral cortices, including the hippocampus (Supplementary Fig. 1a,b). However, body weight trajectories were similar to control mice up to 11 weeks of age, indicative of normal structural development (Supplementary Fig. 1c) and obviating the effects of obesity on the observed group differences described below. We did not observe any significant differences in open-field locomotor activity (Fig. 1b), pre-pulse inhibition (PPI; a measure of sensory-motor gating) (Fig. 1d), and object location performance (used as a test of working memory) (Fig. 1e) among CTL, Env, and Gen groups. However, G × E mice exhibited greater locomotor activity, impaired PPI, and working memory deficits compared with CTL mice (Fig. 1b, d, e). A decline in acoustic startle responses was observed in *Glo1* heterozygous mice fed either diet compared with WTs (Fig. 1c). In contrast, self-grooming, nest building, and elevated plus maze activity (a measure of general anxiety) were influenced by diet but not *Glo1* genotype (Fig. 1f, g, and Supplementary Fig. 2a). No differences were detected in social interaction among groups (Supplementary Fig. 2b).

Sugar is a powerful natural reward, and excessive intake during critical periods of brain development may produce irreversible changes in brain reward system function, including nucleus accumbens (NAc) activity, leading to marked changes in cognitive and behavioral control(*21-24*). Dopamine (DA) elevation within the NAc causes hyper-locomotion among mice(*25*), whereas DA depletion within the NAc suppresses amphetamine-induced hyperactivity(*26, 27*). Moreover, odds ratios for measures of mental distress, hyperactivity, and conduct problems were highest in adolescents who self-reported the greatest levels of soft drink consumption(*28*). Higher basal DA and greater amphetamine-induced release in the striatum are also cardinal characteristic of SZ(*29, 30*). Therefore, we measured DA release in the NAc of our model mice using *in vivo* microdialysis and found both enhanced basal and amphetamine-induced release only in G × E mice (Fig. 1h). Next, to assess whether this enhanced DA release induced the observed behavioral phenotypes, we examined the behavioral effects of aripiprazole, a D2 receptor partial agonist and clinical antipsychotic[35], administered during the last 7 days (0.5 mg/kg/day) of sucrose feeding (Fig. 1a, i–k, and Supplementary Fig. 2c–f). Indeed, the hyper-locomotion and increased striatal DA release observed in G × E mice were completely reversed by aripiprazole treatment (Fig. 1h, i). Moreover, the PPI and working memory deficits observed in G × E mice were also partially improved by

aripiprazole administration (Fig. 1j, k). Conversely, the abnormalities in self-grooming, elevated plus maze activity, and nest building, phenotypes influenced only by diet, were not improved by aripiprazole treatment (Supplementary Fig.2 d–f). Therefore, aripiprazole treatment selectively improved abnormalities associated with dysregulated DA signaling in our model mouse.

Dysfunction of parvalbumin-positive inhibitory interneurons in G × E mice

The precisely coordinated activity of parvalbumin (PV)-positive GABAergic interneurons is crucial for the maintenance of PPI and working memory; moreover, PV neuron hypofunction induces hypersensitivity of dopaminergic neurons to psychostimulants such as amphetamine(*31-34*). We first examined the expression levels of PV by immunohistochemistry and Western blotting to examine if altered PV interneuron activity contributes to these psychiatric disease-associated phenotypes. The number of PV-positive cells was clearly lower in the hippocampus of sucrose-fed mice compared with starch-fed mice (Fig. 2a, b) and lowest in G × E mice (Fig. 2c, d). We measured gamma oscillations (30–45 Hz) by surface electroencephalography (EEG) as gamma oscillations are produced by synchronous activation of PV neurons to examine if this downregulation of PV was accompanied by functional abnormalities

in neural activity. Increased gamma oscillation power is observed in the visual cortex and prefrontal cortex of animals(*35, 36*) and humans(*37-39*) during a variety of perceptual and cognitive tasks, and indeed such increases were observed in Ctrl, Env, and Gen groups. Consistent with PV interneuron dysfunction, however, G × E mice did not exhibit an increase in the gamma oscillation power when approaching a novel object (Fig. 2e, f). Sucrose-fed mice also exhibited elevated baseline gamma oscillation power compared with starch-fed mice in the home cage (Fig. 2e). These results are consistent with findings from SZ and BD patients as well as other mouse models of psychosis showing increased baseline gamma oscillations and decreased sensory stimulus-evoked gamma power(*34, 40-43*). Therefore, our results suggest that G × E mice mimic the pathophysiological changes of PV neurons observed in psychiatric disorders.

To summarize, administration of a high-sucrose diet to *Glo1* heterozygous mice induces behavioral, histological, and pathophysiological phenotypes of psychiatric disorders, suggesting that excessive sucrose intake during adolescence may be a potential environmental risk factor.

AGE accumulation and impaired astrocyte function in G × E mice

We first assessed neurocellular abnormalities associated with reduced GLO1 expression to investigate the mechanisms underlying the emergence of these psychiatric phenotypes, especially in G × E mice. The strongest GLO1 expression was detected in astrocytes, especially those surrounding capillaries (Supplementary Fig. 3a–f). In contrast, we observed moderate GLO1 expression in neurons and weak GLO1 expression in microglia and vascular endothelial cells of heterozygous mice (Supplementary Fig. 3g–i). As expected, GLO1 expression was not detected in the brains of *Glo1* homozygous mice (Supplementary Fig. 3m). Based on this cellular expression prolife, enhanced AGE production or accumulation is expected in the microglia and vascular endothelial cells of mutant mice and especially in G × E mice. Indeed, immunohistochemistry revealed a stronger fluorescent AGE immunoreactive signal (detected using an ab23722 antibody) in the vascular endothelial cells of G × E mice compared with CTL mice (Fig. 3a–g). We also detected another AGE (AGE-4), a product of fructose and carbonyl compounds metabolism, in the microglia of sucrose-fed mice. Furthermore, microglial AGE-4 accumulation in sucrose-fed groups was accompanied by a greater number of processes compared with the starch-fed groups (Supplementary Fig. 4a, e), a morphological phenotype identified in mice under chronic stress(*44, 45*).

In general, cellular damage from AGE accumulation is caused by inflammatory responses induced by RAGE activation or by loss of normal protein function following AGE-forming reactions(*46*). Although these processes may alter multiple signaling pathways in both AGE-accumulating cells and surrounding cells(*47*), it is not possible to investigate the expression patterns of all AGEs. Therefore, we focused on astrocytes as these cells express high levels of GLO1 (Supplementary Fig. 3a–f) and demonstrate a well described reactive phenotype in response to pathogenic status including neuroinflammation characterized by enhanced expression of glial fibrillary acid protein (GFAP). Astrocytic activation was examined in mice expressing green fluorescent protein (GFP) under control of the *GFAP* promoter (*48, 49*). Strongly enhanced *GFAP* promoter function was observed in G × E mice, without changes in the number of GFAP-positive astrocytes (Fig. 3h–j), indicating that the astrocytes in G × E mice are in the reactive pre-condition during high-sucrose feeding(*50, 51*). Taken together, AGE accumulation occurs in cells with low GLO1 expression (Fig 3a–g and Supplementary Fig. 3, 4) and astrocytes exhibit pre-inflammatory status in GLO1-deficient mice on a high-sucrose diet (Fig 3h–j).

Microcapillary angiopathy and impaired glucose intake in G × E mice

Vascular endothelial cells and astrocyte end-feet collectively form a blood–brain barrier (BBB) that tightly controls the parenchymal environment and neuronal function by modulating the selective passage of nutrients and various factors. Accumulation of AGEs in endothelium and astrocyte reactivity may therefore impair BBB function. To examine changes in endothelial function, we first conducted transcriptome analysis of the prefrontal cortex (PFC), a region strongly implicated in psychiatric impairments, using microarrays (Fig. 4a, b). The coagulation factor V, which is essential for the production of fibrin from fibrinogen, ranked seventh on the list of transcripts exhibiting more than doubled expression in G × E mice compared with the other three groups (Fig. 4a, Supplementary Table 1, 2). Fibrin controls hemostasis via polymerization with platelets to form blood clots and deposits of this protein are indicative of endothelial abnormality regardless of the nature of the inciting event (i.e., mechanical insult, infection, or immunological derangements)(*52*). For example, in the early stage of endothelial cell impairment, fibrin accumulates in capillaries. We therefore investigated vascular fibrin accumulation by immunohistochemistry and confirmed the presence of significant fibrin accumulation on the vascular lumen side of endothelial cells in the brain capillaries of G × E mice (Fig. 4c–f).

We speculated that the abnormal vascular endothelial cells observed in G × E mice could alter glucose uptake from the plasma into the brain parenchyma. Extracellular concentrations of glucose in the brain parenchyma were measured under three conditions: 1) fasting, 2) 1 h after eating, and 3) 2 h after eating. Glucose in the parenchyma was significantly lower in G × E mice compared with the other groups at 1 h after eating (Fig. 4g). However, there were differences in plasma glucose and fasting plasma insulin levels among the four groups (Fig. 4h, i), indicating that this lower parenchymal glucose in G × E mice is due to reduced uptake across the BBB rather than dysregulation of plasma glucose or insulin signaling.

Protective effects of chronic low-dose aspirin against behavioral abnormalities and angiopathy

Previous reports have shown adjunct non-steroidal anti-inflammatory drug (NSAID) treatment can improve psychiatric disorder scores (*53*-*56*). The NSAID aspirin is used routinely for the prevention and alleviation of vascular-related adverse events associated with high blood pressure, ischemia, and cardiovascular diseases. Thus, we examined whether aspirin treatment can protect against the development of abnormal behaviors in G × E mice (Fig. 1a, Fig. 5a–d and

Supplementary Fig. 5a–c). Indeed, low-dose aspirin (1 mg/kg/day) prevented deficits in working memory and grooming duration among G × E mice (Fig. 5c and Supplementary Fig. 5b) and partially ameliorated hyper-locomotor activity, PPI deficits, poor nest building, and anxiety in the elevated plus maze (Fig. 5a, b, d, and Supplementary Fig. 5c). These behavioral improvements were accompanied by a decrease in endothelial fibrin accumulation (Fig. 5e, f) and a partial restoration of glucose intake into the brain parenchyma (Fig. 5g). Aspirin treatment also prevented the hyper-ramification of microglia (Supplementary Fig. 4a, e). Collectively, these results suggest that the prevention of fibrin accumulation in G × E mice afforded by aspirin treatment improves brain glucose availability required for normal brain function.

Angiopathy in postmortem brains of psychiatric patients with higher brain dysfunction

We compared immunostaining of brain slices from healthy controls and patients with SZ or BD to examine if psychiatric patients also exhibit this angiopathic fibrin accumulation in vascular endothelial cells. Consistent with the G × E mouse model, patients exhibited significantly elevated fibrin accumulation in the vascular endothelium (Fig. 6a-c). Thus, this fibrin-related angiopathy may contribute to disease progression, despite the absence of *GLO1* gene mutation and no specific

evidence for higher sugar intake compared with controls, suggesting vascular damage as a novel and common phenotype of psychiatric illness.

Discussion

We demonstrate that high dietary sucrose consumption during adolescence is a potential risk factor for the development of neurofunctional and behavioral phenotypes related to psychiatric illness, including impaired sensory gating, interneuron dysfunction and altered cortical oscillatory activity, impaired working memory, elevated anxiety, hyperactivity, and greater basal and stimulus-evoked striatal DA release. Second, we identified endothelial fibrin accumulation ("angiopathy") in both model mice expressing these psychiatric-related phenotypes and in the postmortem brains of SZ or BD patients. Third, we observed that glucose intake from the plasma into the brain parenchyma was impaired in model mice, potentially because of this angiopathy. Finally, we found that chronic low-dose aspirin treatment prevented the deposition of fibrin in capillaries, improved glucose transport, and reversed many of the behavioral phenotypes in model mice, suggesting sucrose-induced angiopathy as a seminal pathogenic event in mental illness.

A possible pathogenic mechanism for dietary sucrose-induced toxicity among *GLO1* heterozygous mice is illustrated in Figure 6d. Sucrose consists of glucose and fructose, and fructose has a potential to generate AGEs more readily than an equal amount of glucose. In addition, fructose generates pre-AGE carbonyl compounds such as glyceraldehyde and methylglyoxal(*57*). Moreover, in cerebrospinal fluid, fructose concentration may be controlled by mechanisms distinct from that in plasma, as levels are higher, whereas glucose levels are lower in this compartment compared with plasma(*58, 59*). Fructose-derived pre-AGE carbonyl compounds were presumably rapidly detoxified by GLO1 in astrocytes of WT mice and probably also *Glo1* heterozygous mice as these cells maintain strong GLO1 expression (Supplementary Fig. 3a, b, d–f). Alternatively, endothelial cells and microglia exhibit lower expression levels in WT mice and sparse expression in heterozygotes (Supplementary Fig. 3j, l), which may result in excessive accumulation of carbonyl compounds and AGEs, leading to a pro-inflammatory response in astrocytes via RAGE signaling or cytokine release from microglia(*60*). In turn, this perivascular inflammation could lead to angiopathy and poor glucose uptake, resulting in damage to various neuronal populations such as PV-containing interneurons(*61*) (Fig. 4c-f, h, i). Indeed, abnormal glucose transport was associated with endothelial cell pathology and astrocyte reactivity

predominantly in *Glo1* heterozygous mice fed a high-sucrose diet (Fig. 4g). Furthermore, the anti-inflammatory aspirin protected against the emergence of angiopathy as evidenced by reduced fibrin accumulation, partially restored parenchymal glucose concentration, and prevented many behavioral phenotypes of psychiatric illness, possibly by reducing inflammation and oxidative stress and by preserving PV-positive neuronal function (Fig. 5 and Supplementary Fig. 5).

We generated a mouse model with psychiatric-related phenotypes based on the G × E approach. Our G × E model mice exhibited hyper-locomotion and excessive striatal DA release, both of which were completely reversed by the dose-dependent selective partial D2 receptor agonist aripiprazole (Fig. 1h, i). These abnormalities may be explained by the PV neuron dysfunction observed in G × E mice (Fig. 2). Genetically induced PV neuron-specific hypofunction leads to an elevated excitation to inhibition ratio in the ventral hippocampus[76]. Recent studies have suggested that chronic stress also induces interneuron hypofunction, including of PV neurons, and concomitant hyperactivity of excitatory neurons in the hippocampus, cortex, and amygdala[77]. Hyperactivity of pyramidal neurons in the ventral hippocampus may underlie the aberrant modulation of midbrain DA release after exposure to an adverse environmental stimulus such as amphetamine[76,78,79]. Moreover, the induction of pan-interneuronal hypofunction by

Gad65-Cre-dependent artificial G□i-coupled receptor (hM4Di) expression triggered hyper-locomotion without amphetamine stimulation[35], whereas suppression of amphetamine-induced hyperactivity by aripiprazole was partly dependent on expression of D2 receptors by PV neurons[76]. Therefore, PV neuron dysfunction induced by excessive sucrose intake in *Glo1* heterozygous mice may be a major cause of the DA-dependent hyper-locomotion observed in these animals (Figs. 1h, i, and 2).

This effect of angiopathy on PV neurons in G × E mice (Fig. 4g) may stem from the unique electrophysiological properties of these cells. Parvalbumin-expressing interneurons exhibit a lower input resistance and higher-amplitude rapid after-hyperpolarization than many projection neurons(*62, 63*), and this combination of properties generates higher frequency action potentials than in other neuron types. To maintain this rapid spiking, PV neurons require high energy expenditure as evidenced by mitochondrial and cytochrome c oxidase enrichment (*64*). Therefore, reduced glucose within the brain parenchyma because of angiopathy may preferentially reduce PV neuron activity. Furthermore, robust PV neuron function is required for PPI, working memory, amphetamine-induced hyper-locomotion, dopamine (or 3,4-dihydroxyphenylacetic acid) regulation, and the generation of gamma oscillations(*31, 33, 34, 65, 66*), all of which are

considered core symptoms of psychiatric disorders. Indeed, reduced PV neuron number has been reported in postmortem brains of patients with psychiatric disorders such as SZ and BP(*67-69*). The inhibitory activity of PV neurons is also critical under environmental stress to prevent sequela of excessive excitatory activity such as oxidative stress and inflammation(*61*), pathogenic processes that may be more prominent during the critical adolescent prodromal period before full brain maturation(*70*).

In this study, we identified capillary angiopathy in both G × E mice and the postmortem brains of SZ and BD patients (Fig. 6a-c). Although the angiopathy observed in our model mice was probably caused by the combined high AGE production capacity of fructose (*71, 72*) and GLO1 deficiency, neither of these conditions were necessarily present in the patient sample. However, a variety of environmental stresses may converge to induce angiopathy. In fact, several studies have reported that stressors such as social defeat, isolation, and viral infection induce vascular defects(*73-75*). Furthermore, these same stressors are SZ and BD risk factors and induce PV neuron hypofunction, which is a core phenotype of these deseases(*76*), suggesting that angiopathy may be a common trigger for psychiatric phenotypes. Patients with SZ and BD also share common genetic risk factors as well as markers of impaired connectivity and cognition (*77*)(*76*). This

vascular impairment may thus be another common feature shared by SZ and BD. Although excessive sugar consumption was not documented in this sample cohort, patients with SZ and BD do consume around two-fold more sugar than age-matched healthy individuals(*78, 79*). More extensive cohort research is warranted to address high dietary sugar as a risk factor for these disorders and associated angiopathy.

Chronic treatment with low-dose aspirin partially mitigated angiopathy (fibrin deposition), impaired glucose transport into the brain parenchyma, and the emergence of most psychiatric disease-associated behavioral phenotypes, including working memory impairment (Fig. 5 and Supplementary Fig. 5). These effects may be attributed to irreversible inhibition of platelet cyclooxygenase-1 (COX-1) activity and thromboxane production, leading to reduced clot formation[96,97] (Fig. 5e, f), and suppression of oxidative stress through inhibition of NADPH oxidase (NOX)-mediated ROS production by endothelial cells and downstream inhibition of the TNF-□-, thrombin-, and AGE-activated transcriptional factor NF-κB[98]. Aspirin also stimulates endothelial nitric oxide synthase (eNOS) activity via lysine acetylation, resulting in the induction of heme oxygenase and a decrease in asymmetrical dimethylarginine. In turn, dimethylarginine serves as an eNOS inhibitor and thus improves the anti-oxidative potential of vascular cells[99-102]

and may prevent positive feedback between AGE and ROS production in our model mice[11,12]. As oxidative stress is a common characteristic of psychiatric disorders[15-17], aspirin may provide protection against disease pathogenesis.

The high-sucrose diet also induced several abnormal phenotypes even in WT mice, including moderately impaired working memory and nest building, excessively prolonged grooming, reduced numbers of PV neurons, and elevated gamma oscillation power in the home cage (Fig. 1e–g, 2a–e). Therefore, a high-sugar diet during adolescence may adversely influence high brain function even in the absence of genetic factors predisposing to serious mental illness.

References and Notes:

1. *Sugar Intake for adults and children* (2015).
2. N. Fidler Mis *et al.*, Sugar in Infants, Children and Adolescents: A Position Paper of the European Society for Paediatric Gastroenterology, Hepatology and Nutrition Committee on Nutrition. *J Pediatr Gastroenterol Nutr* **65**, 681-696 (2017).
3. R. C. Kessler *et al.*, Lifetime prevalence and age-of-onset distributions of DSM-IV disorders in the National Comorbidity Survey Replication. *Arch Gen Psychiatry* **62**, 593-602 (2005).
4. H. Hafner *et al.*, The epidemiology of early schizophrenia. Influence of age and gender on onset and early course. *Br J Psychiatry Suppl*, 29-38 (1994).

5. N. J. Brandon, A. Sawa, Linking neurodevelopmental and synaptic theories of mental illness through DISC1. *Nat Rev Neurosci* **12**, 707-722 (2011).

6. J. L. Wautier *et al.*, Advanced glycation end products (AGEs) on the surface of diabetic erythrocytes bind to the vessel wall via a specific receptor inducing oxidant stress in the vasculature: a link between surface-associated AGEs and diabetic complications. *Proc Natl Acad Sci U S A* **91**, 7742-7746 (1994).

7. C. M. Sena *et al.*, Methylglyoxal promotes oxidative stress and endothelial dysfunction. *Pharmacol Res* **65**, 497-506 (2012).

8. W. Cai, J. C. He, L. Zhu, C. Lu, H. Vlassara, Advanced glycation end product (AGE) receptor 1 suppresses cell oxidant stress and activation signaling via EGF receptor. *Proc Natl Acad Sci U S A* **103**, 13801-13806 (2006).

9. M. Aragno, R. Mastrocola, Dietary Sugars and Endogenous Formation of Advanced Glycation Endproducts: Emerging Mechanisms of Disease. *Nutrients* **9**, (2017).

10. T. Miyata, Alterations of non-enzymatic biochemistry in uremia, diabetes, and atherosclerosis ("carbonyl stress"). *Bull Mem Acad R Med Belg* **157**, 189-196; discussion 196-188 (2002).

11. A. Ciobica, M. Padurariu, I. Dobrin, C. Stefanescu, R. Dobrin, Oxidative stress in schizophrenia - focusing on the main markers. *Psychiatr Danub* **23**, 237-245 (2011).

12. E. Kim *et al.*, Validation of oxidative stress assay for schizophrenia. *Schizophr Res* **212**, 126-133 (2019).

13. B. K. Bitanihirwe, T. U. Woo, Oxidative stress in schizophrenia: an integrated approach. *Neurosci Biobehav Rev* **35**, 878-893 (2011).

14. A. R. Rosa *et al.*, Altered plasma glutathione levels in bipolar disorder indicates higher oxidative stress; a possible risk factor for illness onset despite normal brain-derived neurotrophic factor (BDNF) levels. *Psychol Med* **44**, 2409-2418 (2014).

15. L. G. Nucifora *et al.*, Reduction of plasma glutathione in psychosis associated with schizophrenia and bipolar disorder in translational psychiatry. *Transl Psychiatry* **7**, e1215 (2017).

16. P. J. Thornalley *et al.*, Quantitative screening of advanced glycation endproducts in cellular and extracellular proteins by tandem mass spectrometry. *Biochem J* **375**, 581-592 (2003).
17. P. J. Thornalley, Glutathione-dependent detoxification of alpha-oxoaldehydes by the glyoxalase system: involvement in disease mechanisms and antiproliferative activity of glyoxalase I inhibitors. *Chem Biol Interact* **111-112**, 137-151 (1998).
18. M. Fujimoto *et al.*, Reduced expression of glyoxalase-1 mRNA in mood disorder patients. *Neurosci Lett* **438**, 196-199 (2008).
19. M. Miyashita *et al.*, Clinical features of schizophrenia with enhanced carbonyl stress. *Schizophr Bull* **40**, 1040-1046 (2014).
20. M. Toyosima *et al.*, Schizophrenia with the 22q11.2 deletion and additional genetic defects: case history. *Br J Psychiatry* **199**, 245-246 (2011).
21. R. F. Smith, Animal models of periadolescent substance abuse. *Neurotoxicol Teratol* **25**, 291-301 (2003).
22. L. F. Vendruscolo, A. B. Gueye, M. Darnaudery, S. H. Ahmed, M. Cador, Sugar overconsumption during adolescence selectively alters motivation and reward function in adult rats. *PLoS One* **5**, e9296 (2010).
23. S. D. Iñiguez *et al.*, Nicotine exposure during adolescence induces a depression-like state in adulthood. *Neuropsychopharmacology* **34**, 1609-1624 (2009).
24. E. Zamberletti *et al.*, Alterations of prefrontal cortex GABAergic transmission in the complex psychotic-like phenotype induced by adolescent delta-9-tetrahydrocannabinol exposure in rats. *Neurobiol Dis* **63**, 35-47 (2014).
25. R. D. Oades, K. Taghzouti, J. M. Rivet, H. Simon, M. Le Moal, Locomotor activity in relation to dopamine and noradrenaline in the nucleus accumbens, septal and frontal areas: a 6-hydroxydopamine study. *Neuropsychobiology* **16**, 37-42 (1986).
26. P. H. Kelly, P. W. Seviour, S. D. Iversen, Amphetamine and apomorphine responses in the rat following 6-OHDA lesions of the nucleus accumbens septi and corpus striatum. *Brain Res* **94**, 507-522 (1975).

27. G. F. Koob, L. Stinus, M. Le Moal, Hyperactivity and hypoactivity produced by lesions to the mesolimbic dopamine system. *Behav Brain Res* **3**, 341-359 (1981).

28. L. Lien, N. Lien, S. Heyerdahl, M. Thoresen, E. Bjertness, Consumption of soft drinks and hyperactivity, mental distress, and conduct problems among adolescents in Oslo, Norway. *Am J Public Health* **96**, 1815-1820 (2006).

29. O. D. Howes *et al.*, Molecular imaging studies of the striatal dopaminergic system in psychosis and predictions for the prodromal phase of psychosis. *Br J Psychiatry Suppl* **51**, s13-18 (2007).

30. M. Laruelle *et al.*, Single photon emission computerized tomography imaging of amphetamine-induced dopamine release in drug-free schizophrenic subjects. *Proc Natl Acad Sci U S A* **93**, 9235-9240 (1996).

31. R. Nguyen, Investigating the Roles of Parvalbumin and Cholecystokinin Interneurons of the Ventral Hippocampus and Medial Prefrontal Cortex in Schizophrenia-Related Behaviours. (2018).

32. A. J. Murray *et al.*, Parvalbumin-positive interneurons of the prefrontal cortex support working memory and cognitive flexibility. *Sci Rep* **5**, 16778 (2015).

33. K. Fujihara *et al.*, Glutamate Decarboxylase 67 Deficiency in a Subset of GABAergic Neurons Induces Schizophrenia-Related Phenotypes. *Neuropsychopharmacology* **40**, 2475-2486 (2015).

34. T. Korotkova, E. C. Fuchs, A. Ponomarenko, J. von Engelhardt, H. Monyer, NMDA receptor ablation on parvalbumin-positive interneurons impairs hippocampal synchrony, spatial representations, and working memory. *Neuron* **68**, 557-569 (2010).

35. G. Nase, W. Singer, H. Monyer, A. K. Engel, Features of neuronal synchrony in mouse visual cortex. *J Neurophysiol* **90**, 1115-1123 (2003).

36. K. K. Cho *et al.*, Gamma rhythms link prefrontal interneuron dysfunction with cognitive inflexibility in Dlx5/6(+/-) mice. *Neuron* **85**, 1332-1343 (2015).

37. G. P. Krishnan *et al.*, Steady state visual evoked potential abnormalities in schizophrenia. *Clin Neurophysiol* **116**, 614-624 (2005).

38. R. Y. Cho, R. O. Konecky, C. S. Carter, Impairments in frontal cortical gamma synchrony and cognitive control in schizophrenia. *Proc Natl Acad Sci U S A* **103**, 19878-19883 (2006).

39. M. J. Minzenberg *et al.*, Gamma oscillatory power is impaired during cognitive control independent of medication status in first-episode schizophrenia. *Neuropsychopharmacology* **35**, 2590-2599 (2010).

40. M. Carlen *et al.*, A critical role for NMDA receptors in parvalbumin interneurons for gamma rhythm induction and behavior. *Mol Psychiatry* **17**, 537-548 (2012).

41. E. N. Billingslea *et al.*, Parvalbumin cell ablation of NMDA-R1 causes increased resting network excitability with associated social and self-care deficits. *Neuropsychopharmacology* **39**, 1603-1613 (2014).

42. P. J. Uhlhaas, W. Singer, Abnormal neural oscillations and synchrony in schizophrenia. *Nat Rev Neurosci* **11**, 100-113 (2010).

43. M. I. Atagun, Brain oscillations in bipolar disorder and lithium-induced changes. *Neuropsychiatr Dis Treat* **12**, 589-601 (2016).

44. S. Hellwig *et al.*, Altered microglia morphology and higher resilience to stress-induced depression-like behavior in CX3CR1-deficient mice. *Brain Behav Immun* **55**, 126-137 (2016).

45. S. A. Rowson *et al.*, Neuroinflammation and Behavior in HIV-1 Transgenic Rats Exposed to Chronic Adolescent Stress. *Front Psychiatry* **7**, 102 (2016).

46. M. P. Wautier *et al.*, Activation of NADPH oxidase by AGE links oxidant stress to altered gene expression via RAGE. *Am J Physiol Endocrinol Metab* **280**, E685-694 (2001).

47. M. Toyoshima *et al.*, Enhanced carbonyl stress induces irreversible multimerization of CRMP2 in schizophrenia pathogenesis. *Life Sci Alliance* **2**, (2019).

48. R. Suzuki *et al.*, Expression of the receptor for pituitary adenylate cyclase-activating polypeptide (PAC1-R) in reactive astrocytes. *Brain Res Mol Brain Res* **115**, 10-20 (2003).

49. R. Suzuki *et al.*, A transgenic mouse model for the detailed morphological study of astrocytes. *Neurosci Res* **47**, 451-454 (2003).

50. A. Das *et al.*, Hippocampal tissue of patients with refractory temporal lobe epilepsy is associated with astrocyte activation, inflammation, and altered expression of channels and receptors. *Neuroscience* **220**, 237-246 (2012).

51. D. D. Mao *et al.*, Effect of Qingxin Kaiqiao Fang on Hippocampus mRNA Expression of the Inflammation-Related Genes IL-1beta, GFAP, and Abeta in an Alzheimer's Disease Rat Model. *Evid Based Complement Alternat Med* **2018**, 9267653 (2018).

52. J. P. Luyendyk, J. G. Schoenecker, M. J. Flick, The multifaceted role of fibrinogen in tissue injury and inflammation. *Blood* **133**, 511-520 (2019).

53. N. Muller *et al.*, Celecoxib treatment in an early stage of schizophrenia: results of a randomized, double-blind, placebo-controlled trial of celecoxib augmentation of amisulpride treatment. *Schizophr Res* **121**, 118-124 (2010).

54. M. Nitta *et al.*, Adjunctive use of nonsteroidal anti-inflammatory drugs for schizophrenia: a meta-analytic investigation of randomized controlled trials. *Schizophr Bull* **39**, 1230-1241 (2013).

55. J. Savitz *et al.*, Minocycline and aspirin in the treatment of bipolar depression: a protocol for a proof-of-concept, randomised, double-blind, placebo-controlled, 2x2 clinical trial. *BMJ Open* **2**, e000643 (2012).

56. P. Stolk *et al.*, Is aspirin useful in patients on lithium? A pharmacoepidemiological study related to bipolar disorder. *Prostaglandins Leukot Essent Fatty Acids* **82**, 9-14 (2010).

57. A. Sakasai-Sakai, T. Takata, J. I. Takino, M. Takeuchi, Impact of intracellular glyceraldehyde-derived advanced glycation end-products on human hepatocyte cell death. *Sci Rep* **7**, 14282 (2017).

58. J. J. Hwang *et al.*, The human brain produces fructose from glucose. *JCI Insight* **2**, e90508 (2017).

59. J. J. Hwang *et al.*, Fructose levels are markedly elevated in cerebrospinal fluid compared to plasma in pregnant women. *PLoS One* **10**, e0128582 (2015).

60. Y. Shinozaki *et al.*, Transformation of Astrocytes to a Neuroprotective Phenotype by Microglia via P2Y1 Receptor Downregulation. *Cell Rep* **19**, 1151-1164 (2017).

61. P. Steullet *et al.*, Oxidative stress-driven parvalbumin interneuron impairment as a common mechanism in models of schizophrenia. *Mol Psychiatry* **22**, 936-943 (2017).

62. Y. Kawaguchi, Y. Kubota, GABAergic cell subtypes and their synaptic connections in rat frontal cortex. *Cereb Cortex* **7**, 476-486 (1997).

63. Y. Kawaguchi, H. Katsumaru, T. Kosaka, C. W. Heizmann, K. Hama, Fast spiking cells in rat hippocampus (CA1 region) contain the calcium-binding protein parvalbumin. *Brain Res* **416**, 369-374 (1987).

64. O. Kann, The interneuron energy hypothesis: Implications for brain disease. *Neurobiol Dis* **90**, 75-85 (2016).

65. E. Tomasella *et al.*, Deletion of dopamine D2 receptors from parvalbumin interneurons in mouse causes schizophrenia-like phenotypes. *Proc Natl Acad Sci U S A* **115**, 3476-3481 (2018).

66. G. Buzsaki, A. Draguhn, Neuronal oscillations in cortical networks. *Science* **304**, 1926-1929 (2004).

67. C. L. Beasley, G. P. Reynolds, Parvalbumin-immunoreactive neurons are reduced in the prefrontal cortex of schizophrenics. *Schizophr Res* **24**, 349-355 (1997).

68. T. Hashimoto *et al.*, Gene expression deficits in a subclass of GABA neurons in the prefrontal cortex of subjects with schizophrenia. *J Neurosci* **23**, 6315-6326 (2003).

69. M. Thompson, C. S. Weickert, E. Wyatt, M. J. Webster, Decreased glutamic acid decarboxylase(67) mRNA expression in multiple brain areas of patients with schizophrenia and mood disorders. *J Psychiatr Res* **43**, 970-977 (2009).

70. T. R. Insel, Rethinking schizophrenia. *Nature* **468**, 187-193 (2010).

71. A. Gugliucci, Formation of Fructose-Mediated Advanced Glycation End Products and Their Roles in Metabolic and Inflammatory Diseases. *Adv Nutr* **8**, 54-62 (2017).

72. J. Chaudhuri *et al.*, The Role of Advanced Glycation End Products in Aging and Metabolic Diseases: Bridging Association and Causality. *Cell Metab* **28**, 337-352 (2018).

73. C. Menard *et al.*, Social stress induces neurovascular pathology promoting depression. *Nat Neurosci* **20**, 1752-1760 (2017).

74. W. A. Banks *et al.*, Lipopolysaccharide-induced blood-brain barrier disruption: roles of cyclooxygenase, oxidative stress, neuroinflammation, and elements of the neurovascular unit. *J Neuroinflammation* **12**, 223 (2015).

75. D. Ben-Nathan, S. Lustig, H. D. Danenberg, Stress-induced neuroinvasiveness of a neurovirulent noninvasive Sindbis virus in cold or isolation subjected mice. *Life Sci* **48**, 1493-1500 (1991).

76. D. Koshiyama *et al.*, White matter microstructural alterations across four major psychiatric disorders: mega-analysis study in 2937 individuals. *Mol Psychiatry*, (2019).

77. S. M. Purcell *et al.*, Common polygenic variation contributes to risk of schizophrenia and bipolar disorder. *Nature* **460**, 748-752 (2009).

78. J. C. Ratliff *et al.*, The effect of dietary and physical activity pattern on metabolic profile in individuals with schizophrenia: a cross-sectional study. *Compr Psychiatry* **53**, 1028-1033 (2012).

79. J. L. Elmslie, J. I. Mann, J. T. Silverstone, S. M. Williams, S. E. Romans, Determinants of overweight and obesity in patients with bipolar disorder. *J Clin Psychiatry* **62**, 486-491; quiz 492-483 (2001).

80. A. V. Kalueff *et al.*, Neurobiology of rodent self-grooming and its value for translational neuroscience. *Nat Rev Neurosci* **17**, 45-59 (2016).

81. P. Jirkof, Burrowing and nest building behavior as indicators of well-being in mice. *J Neurosci Methods* **234**, 139-146 (2014).

82. C. S. Pedersen, D. B. Sorensen, A. I. Parachikova, N. Plath, PCP-induced deficits in murine nest building activity: employment of an ethological rodent behavior to mimic negative-like symptoms of schizophrenia. *Behav Brain Res* **273**, 63-72 (2014).

83. A. Forsingdal, K. Fejgin, V. Nielsen, T. Werge, J. Nielsen, 15q13.3 homozygous knockout mouse model display epilepsy-, autism- and schizophrenia-related phenotypes. *Transl Psychiatry* **6**, e860 (2016).

84. A. Ennaceur, J. Delacour, A new one-trial test for neurobiological studies of memory in rats. 1: Behavioral data. *Behav Brain Res* **31**, 47-59 (1988).

85. L. A. Tellez *et al.*, Separate circuitries encode the hedonic and nutritional values of sugar. *Nat Neurosci* **19**, 465-470 (2016).

86. W. T. Golde, P. Gollobin, L. L. Rodriguez, A rapid, simple, and humane method for submandibular bleeding of mice using a lancet. *Lab Anim (NY)* **34**, 39-43 (2005).

Acknowledgments: We would like to thank MS. Sayaka Ogikubo, MS, Yoshie Matsumoto, MS. Haimei Zhang and MS. Minami Murata, Izumi Nohara, Yukiko Shimada, Emiko Hama, Nanako Obata, Mai Hatakenaka, Chikako Ishida for their contribution to help us with experiments related to this research. We also thank Dr. Tohru Kodama for teaching us about microdialysis and encephalogram recording, Dr. Jun Horiuchi and Dr. Kenji Tanaka for review the study, Ms. Chiaki Watanabe and Ms. Hiromi Onuma for their contribution to coordinating donations of postmortem brains, Prof. Hideki Chiba for the preparation of postmortem brain samples. We also express our gratitude to the families of the deceased for the donations of brain tissue and their time and effort devoted to the consent process and interviews.

Funding: This work was supported by Japan Society for the Promotion of Science KAKENHI Grant 18K14832 (to S.H.), 17K18395, 19K08033 (to H.M.), 17K16408 (to T.T.), 18H02537, 18K19383 (to H.O.) and also by the Ichiro Kanehara Foundation, the Japan Prize Foundation and the Takeda Science Foundation (to S.H.), Strategic Research Program for Brain Sciences from AMED Grant JP19dm0107107 (to H.Y.), and Grant-in-Aid for Scientific Research on Innovative Areas from the MEXT JP16H06277 (to H.Y.). This research was also supported by KAKENHI Grant Numbers: 16H05380（to M.A.）, 18K06977（to K.T.）19H03589（to M.I.）, 18K15354（to K.S.）, AMED Grant Number: JP19dm0107088（to M.I.）, The Kanae Foundation for the Promotion of Medical Science（to K.T.）and The Uehara Memorial Foundation（to M.A.）.

Author contributions: S.H. and H.O. designed the study. S.H. performed and analyzed all experiments. H.M. helped with experimental design of EEG recording and analysis of the results, and edited the manuscript. T.T. coordinated the EEG recording. Y.K., M.H., R.I., A.N., and H.Y. helped with the design of experiments using human specimens and provided fixed human brain sections. T.N. and S.S. provided GFAP-GFP mice. T.D. and T.M. generated and provided *Glo1* knockout (KO) mouse. K.T. and K.S. backcrossed *Glo1* KO mice to B6J mice for all experiments.

Y.N. performed cDNA microarray analysis of gene expression. M.I., M.A., K.T., K.S. and M.M. helped this study with important suggestions. S.H. generated all figures, tables, and wrote the manuscript. H.O. edited the manuscript and supervised this study.

Competing interests: Authors declare no competing interests.

Data and materials availability: All materials used in this paper are available if you request. See Material and Method section if you need the accession number for transcriptome analysis data.

Supplementary Materials:

Materials and Methods

Animals

All experimental procedures were approved by the Animal Experimentation Ethics Committee of the Tokyo Metropolitan Institute of Medical Science (49040). All mice were maintained under a 12:12 h light:dark cycle (lights on at 8:00 AM) with free access to the indicated diet. All efforts were made to minimize the number of animals used and their suffering. The generation of *Glo1* knockout mice will be described in a future publication. In brief, *Glo1*-trapped ES cell lines from

the International Gene Trap Consortium were used for the generation of three founder mice, which were then backcrossed to C57BL/6 mice. Alternatively, mice were backcrossed to GFAP-GFP mice to monitor the activation of astrocytes[50,51]. Male mice were used exclusively in the behavioral tests, whereas mice of both sexes were used in histological, biochemical, and physiological experiments.

Diet preparation

The two diets used in this study were newly created in collaboration with Oriental Yeast Co., Ltd. (Tokyo, Japan). We named the sucrose diet HSD-70 (# OYC 2405100) and the starch diet HCD-70 (# OYC 2405000) (Supplementary Table 4). They contain the same caloric proportions of carbohydrate, fat, and protein, but all carbohydrate calories are derived from either starch or sucrose.

Drug preparation

Aripiprazole was dissolved in acetic acid and diluted to 3.5 mg/L in water for administration at 0.5 mg/kg/day. The final acetic acid concentration in the drinking water was 0.7%. Aspirin was

dissolved in ethanol and diluted to 70 mg/L in water for administration at 1 mg/kg/day. The final ethanol concentration in the drinking water was 0.15%. The daily dose was based on an assumed average water consumption of 5 mL per day.

Behavioral tests

Mice were habituated in the behavioral room for over 30 min before each test. Behavioral tests were performed in the following sequence of increasing stress: elevated plus maze, grooming, nest building, open field, object location, social interaction, and PPI. All test apparatuses were cleaned with 70% ethanol and water between trials, and the subsequent test session was started only after the ethanol vapor odors had disappeared and the apparatuses had dried.

The elevated plus maze (EPM-04M, Muromachi, Japan) consisted of two opposing open arms (297 × 54 mm) and two closed arms (300 × 60 × 150 mm) extending from a central platform (60 × 60 mm). The entire apparatus was elevated 400 mm above the floor. Each mouse was placed on the central platform facing a closed arm and allowed to explore the maze freely for 10 min. Arm entry was defined as the entry of all four paws into the arm. The time spent in the open arms over 10 min was recorded as an index of state anxiety.

For the self-grooming test, all mice housed in the same home cage were moved into a new cage for 10 min. Each mouse was then placed individually in a standard mouse home cage (31 × 16.5 × 14 cm) illuminated at ~200 lux. After a 10 min habituation period, each mouse was scored for cumulative time spent grooming all body regions(*80*) over 10 min using a stopwatch. Self-grooming behavior is conserved across species and is indicative of certain pathological conditions or factors. In humans, for example, self-grooming increases during stressful conditions and in certain psychiatric disorders(*80*).

For the nest building test, 200 g of corncob was spread across the bottom of each cage for bedding, and a square-shaped piece of cotton was placed in the cage center as raw material for the nest. Each subject was placed individually in the cage for 8 h. Photos of the constructed nest were acquired every 2 h, and the nest building process was evaluated by measuring the proportion of loose cotton as follows: one point for 25% weight (Wt%) loosened, two points for 50 Wt% loosened, three points for 75 Wt% loosened, and four points for 100 Wt% loosened. After 8 h, we checked the shape of the nest and added one point if the mice had completed a nest with a bird's nest-like shape. The temperature of the room was maintained at 25°C and illumination at 150–180

lux during nest building. Nest building behavior is an indicator of general well-being in mice(*81*), whereas poor nest building is an indicator of psychological or physiological abnormalities(*82*, *83*). For the open field (OF) test, each mouse was placed in the center of the apparatus ($40 \times 40 \times 40$ cm; 150–180 lux illumination) and allowed to move freely for 10 min. The behavior of each mouse was monitored using a Charge Coupled Device (CCD) camera mounted on the ceiling above the OF. The total distance traveled (cm) was measured using CompACT VAS software (Muromachi).

For the object location test (OLT) of working memory(*84*), mice first explored the empty OF box, and then, two identical objects A and B (two 500 mL PET bottles filled with blue-colored water) were placed in two corners 5 cm from the wall. After a 10 min exploration/learning period, the mice were returned to their home cage for 5 min, and Object A was moved to a new corner (Object A′). The animals were then placed back in the OF box and allowed to explore for 5 min. The time spent exploring A′ and B were measured to calculate a discrimination index representing working memory according to the following equation: Discrimination Index = (Novel Object A′ exploration time − Familiar Object B exploration time) / (Novel Object A′ + Familiar Object B exploration times). The OLT was performed under illumination at 10–15 lux.

The social interaction test was conducted as described [87] using a specialized Sociability Apparatus (SC-03M, Muromachi). The time spent sniffing a novel stimulus mouse or object was manually scored from videos recorded using an overhead color USB camera (aa000080a02, Iroiro House). Stimulus mice (129Sv/SvJcl strain) matched to test mice for age and sex were habituated to the apparatus and to the enclosure cup for 30 min per day for 2 days prior to testing. The location (left or right) of the novel object and novel mouse within an enclosure were alternated across test subjects. The test mouse was allowed to acclimate to the apparatus for a total of 20 min before the sociability test, the first 10 min in the central chamber with the doors closed and then for 10 min in the empty arena with the doors open. The test subject was then briefly confined to the center chamber while a novel stimulus mouse in an enclosure cup was placed on one of the side chamber, with another empty enclosure cup (novel object) was placed on the other side of the chamber. The test subject was allowed to approach the novel object or mouse freely for 10 min. The time spent interacting with the stimulus mouse versus the novel object was calculated as an index of sociability.

The SR-LAB-Startle Response System (San Diego Instruments) was used to detect acoustic startle reflexes and pre-pulse inhibition (PPI). Startle responses were measured using five stimulus

intensities (80, 90, 100, 110, and 120 dB) delivered 10 times each for 40 ms over a white noise background (65 dB). The stimuli were presented in quasi-random order at random inter-trial intervals (10–20 s). In the PPI session, mice were exposed to two stimulus patterns: 1) a startle stimulus alone (120 dB, 40 ms) with no pre-pulse stimulus and 2) a startle stimulus (120 dB, 40 ms) following a pre-pulse stimulus (70 dB for 20 ms; lead time, 100 ms). Each trial was repeated 10 times in quasi-random order at random inter-trial intervals (10–20 s). PPI was defined as the percent decline in startle response because of pre-pulse stimuli according to the following equation: 100 − [(120 dB startle amplitude after any pre-pulse) / (120 dB startle amplitude only)] × 100.

Immunohistochemistry

After transcardial perfusion with PBS and 4% paraformaldehyde, whole brains were collected, post-fixed at 4°C overnight, and then cryoprotected in 20% sucrose at 4°C overnight. Serial coronal sections (50 μm) were then cut using a cryostat (CM3050 S; Leica Microsystems). The antigens in the tissues were reactivated by heating in HistoVT One solution (Nakalai Tesque) for 30 min at 70°C using a water bath. Sections were permeabilized with 0.2% Triton X-100 and 1%

Block Ace (DS Pharma Biomedical) in PBS for 30 min at room temperature and then incubated overnight with the indicated primary antibodies at room temperature. For immunohistochemistry of postmortem human brain tissues, paraffin blocks including BA9 (a region of frontal cortex) were sliced into 10 μm sections, deparaffinized with xylene, and rehydrated with decreasing concentrations of ethanol in water. Antigens were reactivated by heating in HistoVT One solution for 30 min at 90°C using a water bath. Sections were treated with TrueBlack Lipofuscin Autofluorescence Quencher (Biotium Inc.) for 30 s at room temperature and blocked with 1% Block Ace (DS Pharma Biomedical) in PBS for 30 min at room temperature. Thereafter, mouse and human brain sections were subjected to the same immunostaining procedures. The following primary antibodies were diluted in PBS containing 0.4% Block Ace: goat anti-PV (Frontier Institute, PV-Go-Af860; 1:2000), mouse anti-ALDH1L1 (Abnova, H00010840-M01; 1:200), FITC-conjugated tomato lectin (VECTOR, FL-1171; 1:200), chick anti-GFP (Abcam, ab13970; 1:500), goat anti-IBA1 (Abcam, ab48004; 1:100), mouse anti-NeuN (Millipore, MAB377; 1:500), rabbit anti-AGE (Abcam, ab23722; 1:2000), rabbit anti-IBA1 (Wako, WDJ3047; 1:300), and rabbit anti-fibrin (Dako, A0080, 1:500). Sections were then washed three times with PBS-0.05% Tween-20, incubated for 2 h with fluorochrome-conjugated secondary antibodies in PBS

containing 0.4% Block Ace, and washed an additional three times in PBS containing 0.4% Block Ace. For enhanced horseradish peroxidase (HRP) immunostaining, samples were treated with 3% H_2O_2 in PBS for 20 min after the reactivation step to quench endogenous peroxidase activity and then washed in PBS. Sections were incubated with rabbit anti-GLO1 (Novusbio, NBP2-75514, 1:1500) and/or mouse anti-AGE4 (Trans Genic Inc, 14B5, 1:400), followed by incubation with anti-IgG antibodies conjugated to biotin (Vector, 1:200). After washing as described for other secondary antibodies, sections were incubated with streptavidin-conjugated HRP (Jackson ImmunoResearch, 1:200) for 120 min and washed three times with PBS-0.05% Tween-20. The TSA Plus Fluorescence System (PerkinElmer) was used to detect HRP activity. All preparations were counterstained with DAPI (Nacalai Tesque) to reveal cell nuclei, washed three additional times, mounted in Permaflow (Thermo Scientific), and observed using a FluoView® FV3000 Confocal Laser Scanning Microscope (Olympus). Counting of GFP-, AGE-, AGE4-, and fibrin-positive cells and measurements of immunopositive areas were performed in a fixed area using ImageJ version 2.0.0-rc-59/1.51n.

Immunoblotting

Extracts from mouse hippocampi were homogenized in lysis buffer containing 40 mM Tris base, 0.4% sodium dodecyl sulfate (SDS), 0.01 M EDTA (pH 8.0), 8 M urea, and 1 mM phenylmethylsulfonyl fluoride. The total lysate protein content was quantified using a DC Protein Assay Kit (Bio-Rad). Total protein (30 □g per gel lane) was separated by SDS–PAGE and transferred to PVDF membranes (Millipore). Membranes were blocked with TBST buffer (1.37 M NaCl, 2.7 mM KCl, and 0.25 M Tris, pH 8.0) including 0.2% Triton X-100 and 5% bovine serum albumin (BSA) for 30 min at room temperature with slow shaking, followed by incubation overnight with primary antibodies in TBST including 2% BSA at 4°C. The primary antibodies used were rabbit anti-GLO1 (Santa Cruz, sc-67351; 1:1000), mouse-anti-PV (Swant, PV-235; 1:1000), and mouse-anti-tubulin (Santa Cruz, sc-32293; 1:10000). After washing three times with TBST, membranes were incubated with the secondary antibody (HRP-conjugated anti-mouse or anti-rabbit IgG antibody, GE Healthcare; 1:2000) in TBST plus 2% BSA. After washing three times with TBST, blots were processed for chemiluminescence using standard protocols (ECL Prime Western Blotting Detection Regent #RPN2236, GE Healthcare), and signals were detected with an LAS 4000 Imager (Fuji Film).

Microdialysis

We used an in vivo microdialysis system for measurement of extracellular dopamine concentration(*85*) and for collection of brain parenchymal dialysate. After anesthesia by intraperitoneal injection of ketamine (80 mg/kg)/xylazine (16 mg/kg), mice were fixed in a stereotaxic apparatus (Narishige) and a microdialysis guide cannula (CXG-8, Eicom) was implanted in the medial prefrontal cortex (mPFC) (antero-posterior (AP), +1.8 mm; medio-lateral (ML), ±0.15 mm; dorso-ventral (DV), −1.5 mm from bregma), or nucleus accumbens (NAc) (AP, +1.5 mm; ML, ±0.6 mm; DV, −3.5 mm from bregma). After recovery for at least 10 days, a microdialysis probe (CX-I-8-01 for the mPFC and CX-I-8-02 for NAc; Eicom) was inserted through the guide cannula. After insertion, the probe was connected to a syringe pump and perfusion was performed at 2 μL/min for NAc and 0.5 μL/min for mPFC using Ringer's solution (147 mM NaCl, 4 mM KCl, and 2.3 mM $CaCl_2$). Dialysate samples were collected every 10 min and automatically loaded onto an HTEC-500EPS HPLC unit (Eicom). Constant 5-HT concentration in three consecutive collection periods was first confirmed to rule out blood contamination before starting the dopamine concentration measurements or collection of parenchymal dialysates. Analytes were then separated on an affinity column (PP-ODS III, Eicom),

and compounds were subjected to redox reactions within an electrochemical detection unit (amperometric DC mode; applied potential range, 450 mV). The resulting chromatograms were analyzed using an EPC-500 data processor (Eicom), and actual sample concentrations were computed based on the peak heights obtained using 0.01, 0.1, and 1 pg dopamine in standard solution (Sigma). The locations of the microdialysis probes were then confirmed histologically.

EEG recordings

For behavioral and video/EEG monitoring, mice were anesthetized by intraperitoneal injection of ketamine (80 mg/kg)/xylazine (16 mg/kg), fixed in a stereotaxic apparatus (Narishige, Japan), and implanted with EEG and electromyography (EMG) electrodes. The EEG electrodes were gold-coated stainless steel screws (SUS303) soldered with lead wires (ANE-0190, Adler's Nest, Japan) implanted epidurally over the left frontal cortex (AP, 1 mm; ML, 1 mm) and the bilateral parietal cortex (AP, −2 mm; ML, ±2 mm). All wires were soldered to a multichannel electrical connector (R833-83-006-001, TOKIWA SHOKO, Japan). The left parietal cortex electrode was used as a reference for monitoring the frontal cortex EEG. The EMG electrodes were lead wires placed bilaterally into the trapezius muscle. After recovery for at least 10 days, EEG/EMG signals

were amplified and band-pass filtered (EEG: 1.5–1000 Hz; EGM: 15–3000 Hz) using a MEG-6116 system (NIHON KOHDEN), digitized at a sampling rate of 200 Hz, recorded using a data acquisition system (PowerLab 8/30, ADInstruments), and analyzed using LabChart Software (ADInstruments). Behavioral activities were recorded using a USB camera (aa000080a02, Iroiro House, Japan). Behavioral and electrophysiological responses to a novel object (an empty 100 ml DURAN bin) were recorded in an OF chamber (20 × 20 × 26 cm). The novel object was placed in one corner of the OF chamber to induce exploration. The 30 s preceding first contact with the novel object was analyzed for object recognition ("object activity"). For EEG monitoring in the home cage, mice were first habituated for 8 h. Home cage EEG data were then acquired for 2 min after awaking as confirmed by clear EMG signals and movement images from an offline video camera analysis ("home cage activity"). All recordings were converted into power spectra using a fast Fourier transform (FFT) algorithm with a 5 s Hann cosine-bell window and 50% overlap between successive window measurements. All FFTs were at 1024 points to obtain 0.512 Hz resolution. The total signal amplitude or power (V^2) in each 5 s period was measured as the power magnitude at each frequency. The grouped power spectra were averaged over the following frequency ranges: 1–4 Hz (delta), 5–10 Hz (theta), 30–45 Hz (low gamma), and 55–80 Hz (high

gamma). The power values detected at each frequency range for 30 s were further averaged over 30 s of total EEG power using the average values to remove potential noise. These analyses were performed using custom software written in MATLAB (R2019b; MathWorks).

Transcriptome analysis

Three independent total RNA samples from each group were mixed and purified using an RNeasy Mini Kit (Qiagen). RNA quality was assessed using a 2100 bioanalyzer (Agilent Technologies). Cy3-labeled cRNA was prepared using a Low Input Quick Amp Labeling Kit in accordance with the manufacturer's protocol (Agilent Technologies). Samples were hybridized to the SurePrint G3 Mouse Gene Expression v2 Microarray (G4852B; Agilent Technologies). The array was then washed and scanned using the SureScan Microarray Scanner (Agilent Technologies). Microarray images were analyzed using the Feature Extraction software with default settings for all parameters (Agilent Technologies). Data from each microarray analysis were normalized by shift to the 75th percentile without baseline transformation. Microarray results were deposited in the Gene Expression Omnibus database under accession number GSE141829.

Insulin and glucose measurements

Blood plasma was collected from the mouse cheek as described by Golde(*86*). Plasma glucose concentration was measured using a Precision-Neo blood glucose meter (#71386-80, Abbott Japan), plasma insulin concentration using an ELISA kit (#M1102, MORINAGA), and glucose concentration in the dialysate samples using a different ELISA kit (#ab65333, Abcam) all according to the manufacturers' guidelines. Data were collected on a microplate reader (Varioskan, Thermo Fisher Scientific).

Human postmortem brain tissue collection

Postmortem brain tissues from SZ and BD patients were obtained from the Fukushima Brain Bank at the Department of Neuropsychiatry, Fukushima Medical University. Postmortem brain tissues from control subjects were obtained from the Section of Pathology, Fukushima Medical University Hospital. The use of postmortem human brain tissues in this study was approved by the Ethics Committee of Fukushima Medical University (No.1685) and Tokyo Metropolitan Institute of Medical Science (No. 18-20) and complied with the Declaration of Helsinki and its later amendments. All procedures were conducted with the informed written consent of the next of kin.

Detailed demographic information of the 10 subjects with SZ, 9 subjects with BD, and the 12 age- and sex-matched control subjects is provided in **Supplementary Table 3**. There were no between-group differences in sex (Fisher's exact test, Ctrl and SZ: p = 1.00, Ctrl and BD: p =0.40), age (Student's t-test, Ctrl and SZ: p=0.69, Welch's t-test, Ctrl and BD: p= 0.66), postmortem interval (PMI) (Student's t-test, Ctrl and SZ: p = 0.89, Ctrl and BD: p =0.98) and history of diabetes mellitus (Fisher's exact test, Ctrl and SZ: p = 0.59, Ctrl and BD: p =0.59). Each SZ and BD patient fulfilled the diagnostic criteria established by the American Psychiatric Association (Diagnostic and Statistical Manual of Mental Disorders, DSM-IV) and did not have a past history of other neurological disorders or substance abuse. Moreover, none of the control subjects had any record of mental disorders, neurological disorders, or substance abuse.

Statistical analyses

Data were analyzed using the Tukey–Kramer test or two-way repeated-measures ANOVA with post hoc Shaffer's multiple comparisons tests. GLO1 immunoblotting results were compared by Dunnett's test and postmortem brain staining results by Welch's *t*-test. Behavioral results from starch +/+ and Suc *Glo*1/+ groups were reused according to the 3R rule. The number of animals

used can be found in the legend of each figure. Significance was set at $P < 0.05$ (two-tailed) for all tests.

Supplementary Figure Legends

Supplementary Figure 1 Characterization of regional GLO1 expression in WT and heterozygous *Glo1* mutant mice fed starch or sucrose.

(a) Western blot analysis of GLO1 protein expression using tubulin as an internal control. The cerebral cortex, including the hippocampus, was used as the loading sample. (b) Densitometric analysis of GLO1 protein expression (Starch +/+, n = 3; Starch *Glo1*/+, n = 4; Suc +/+, n = 3; Suc *Glo*1/+, n = 4). To quantify expression, the intensities of GLO1 bands shown in a were divided by the intensities of corresponding tubulin bands. (c) Body weight trajectories. No significant differences were observed among groups (n = 9–10 mice per group). Dunnett's test was used in b and two-way repeated-measures ANOVA in c. Main effect of group ($F_{3, 33} = 1.7512$, $P = 0.1757$). The data are presented as the mean ± s.e.m. *$P < 0.05$.

Supplementary Figure 2 Effect of aripiprazole treatment on behavioral phenotypes.

(a) Elevated plus maze test to evaluate anxiety. (b) Interaction time with an empty cylinder (novel object) or a stimulus mouse placed in the cylinder during the social interaction test. No differences were detected in social interaction among the four groups. (c–f) Effects of aripiprazole treatment on the acoustic startle response (c), self-grooming (d), elevated plus maze performance (e), and nest building skill (f). The abnormal behaviors of G × E mice in these tests were not improved by aripiprazole treatment. The Tukey–Kramer test was used in a, b, d, and e, whereas two-way repeated-measures ANOVA was used in c and f. Main effects of group are as follows: c ($F2, 35 = 8.557$, $P = 0.0009$) and f ($F2, 47 = 14.6637$, $P = 0.004$). The data are presented as the mean ± s.e.m. $^{*}P < 0.05$; $^{**}P < 0.01$; $^{***}P < 0.001$.

Supplementary Figure 3 Cellular localization of GLO1 in the cerebral cortex of sucrose-fed wild-type mice.

(a–f) Localization of GLO1 in astrocytes. (a) Immunohistological images of GLO1 co-immunostaining with an astrocyte marker (ALDH1L1) or with an endothelial cell marker (tomato lectin). (b) Merged image of GLO1 and ALDH1L1 immunoreactivity in a. The yellow arrows in b indicate cells with colocalization of GLO1 and ALDH1L1. (c) Merged image of GLO1

and lectin from a. The white arrows point to representative GLO1-positive cells located close to the endothelial cells. (d, e) Higher-magnification images of GLO1 co-immunostaining with ALDH1L1 or with tomato lectin from a different focal plane. (e) Merged image of GLO1 and ALDH1L1 from d. (f) Plots of pixel intensities along the yellow arrow in e. The black arrows indicate the areas of GLO1 and ALDH1L1 colocalization. (h) Merged image of GLO1 and tomato lectin from g. (i) Plots of pixel intensities along the white arrow in h. Unlike that observed in f, the GLO1 expression pattern was similar to that of tomato lectin expression, whereas ALDH1L1 exhibited a distinct expression pattern. (j) Co-immunostaining of GLO1 with the neuronal marker NeuN and the microglial marker IBA1. (k) Merged image of GLO1 and NeuN immunoreactivity from j. The yellow arrows indicate neurons with mild GLO1 immunoreactivity. (l) Merged image of GLO1 and IBA1 from j. The white arrows indicate microglia with weak GLO1 immunoreactivity. (m) GLO1 immunostaining together with DAPI staining in *Glo1* homozygous mice.

Supplementary Figure 4 Fructose-derived AGE accumulation in microglia of sucrose-fed mice.

(a, b) Immunohistochemical images of the microglial marker IBA1 and AGE4 in the CA1 region. (c) Merged image of AGE4 and IBA1 immunoreactivity. (d) Higher-magnification images of AGE4 co-immunostaining with IBA1. (e) Number of protrusions in each IBA1-positive cell from a. Mean number of protrusions in five randomly selected cells per image from three independent mice. (f) Measurement of the area covered by AGE immunoexpression in a (defined as the area of pixels above threshold, in which the area is above the appropriate threshold of pixel intensity in each image. The mean intensity of the entire image was measured for each section (one slice from four or five mice). Tukey–Kramer tests were used in e and f. $*P < 0.05$; $**P < 0.01$; $***P < 0.001$.

Supplementary Figure 5 Protective effects of aspirin against the development of abnormal behaviors in G × E mice.

(a–c) Effects of aspirin treatment on the acoustic startle response (a), self-grooming (b), and elevated plus maze performance (c). Aspirin prevented deficits in grooming duration and partially ameliorated the decline in acoustic startle response. It also increased the time spent in the open arms of the elevated plus maze, suggesting reduced anxiety. Two-way repeated-measures

ANOVA was used in a ($F2, 42 = 8.0903$, $P = 0.0011$) and the Tukey–Kramer test in b and c. The data are presented as the mean ± s.e.m. *$P < 0.05$; ***$P < 0.001$.

Fig. 1 Generation of G × E model mice and analyses of psychiatric disease-related phenotypes. (a) Timeline of the experiments. After weaning (P21), wild-type (WT) and *Glo1* heterozygous mutant mice were fed either a starch diet (control) or a sucrose diet (experimental). Diets were equal in total calories and proportions of calories from carbohydrates, lipids, and proteins. The behavioral test battery was administered starting at 2 months of age (upper panel). Middle panel: Macronutrient composition of the two diets. We used *Glo1* heterozygous mice to mimic patients with psychiatric disorders who exhibit decreased GLO1 activity or expression, whereas the high-sucrose intake was used as the environmental risk factor (bottom panel). We investigated four groups of mice: WT, starch-fed mice (Starch +/+); *Glo1* heterozygous, starch-fed mice (Starch *Glo1*/+); WT, sucrose-fed mice (Suc +/+); and *Glo1* heterozygous, sucrose-fed mice (Suc *Glo1*/+). (b–g) Behavioral analyses of the four groups of mice (n = 18–23 mice per group). (b) Spontaneous locomotor activity in the open-field test. (c) Acoustic startle responses. (d) Pre-pulse inhibition (PPI) using a 70 dB pre-pulse. (e) Object location test to evaluate working memory. (f)

Duration of self-grooming in the home cage. (g) Quantification of nest building skills over 8 h. (h) Extracellular concentration of dopamine in the nucleus accumbens (NAc) measured at 20 min intervals using an *in vivo* microdialysis system. Methamphetamine (1.25 mg/kg) was administered by intraperitoneal (i.p.) injection at time 0 (arrow) (n = 8–11 mice per group). (i–k) Effects of aripiprazole (Aripi) treatment on abnormal behaviors (n = 16–18 mice per group). (i) Quantifications of locomotor activity. (j) PPI for the 70 dB pre-pulse. (k) Object location test. Tukey–Kramer test was used in d, e, f, j, and k, whereas two-way repeated-measures ANOVA was used in b, c, g, h, and i. Main effects of group were as follows: b ($F_{3, 73} = 6.19$, $P = 0.0008$), c ($F_{3, 63} = 6.75$, $P = 0.0005$), g ($F_{3, 81} = 6.67$, $P = 0.0004$), h ($F_{4, 36} = 14.0374$), and i ($F_{2, 51} = 27.59$, $P < 0.0001$). These ANOVA tests were followed by Shaffer's multiple comparisons tests for genotype groups. (h) Bonferroni multiple comparisons test of genotype groups at specific time points, ###$P < 0.001$ for Suc *Glo1*/+ vs. Ctrl (Starch +/+), $$$P < 0.01$ for Starch *Glo1*/+ vs. Ctrl (Starch +/+). Data are presented as mean ± s.e.m. *$P < 0.05$, **$P < 0.01$, ***$P < 0.001$; n.s., not significant.

Fig. 2 Parvalbumin-positive interneuron dysfunction in G × E mice.

(a) Immunohistochemistry of parvalbumin (PV) in the hippocampal dentate gyrus (DG). (b) Number of PV-positive cells in the DG (average of one slice from three mice per group). (c) Western blot analysis of PV protein expression using tubulin as the internal control. (d) Densitometric analysis of PV protein expression. To quantify expression, PV band intensities were divided by corresponding tubulin band intensities (n = 3 mice per group). (e) Average gamma band power in the home cage and during novel object recognition in the open field (n = 7–8 mice per group). (f) Changes in gamma band power from the home cage to the novel object phase in individual mice (n = 7–8 mice per group). Tukey–Kramer tests were used in b, d, and e, whereas two-way repeated-measures ANOVA were used in f. The main effects of group were as follows: b ($F_{3, 73} = 6.19$, $P = 0.0008$), c ($F_{3, 63} = 6.75$, $P = 0.0005$), g ($F_{3, 81} = 6.67$, $P = 0.0004$), h ($F_{4, 36} = 14.0374$), and i ($F_{2, 51} = 27.59$, $P < 0.0001$). ANOVA tests were followed by Shaffer's multiple comparison tests for genotype groups. Data are presented as mean ± s.e.m. *$P < 0.05$, **$P < 0.01$, ***$P < 0.001$; n.s., not significant.

Fig. 3 AGE accumulation in the neurovascular endothelium and pre-inflammatory status of astrocytes in G × E mice.

(a) Images of AGE immunohistochemistry in the medial prefrontal cortex. (b) Measurement of the area covered by AGE immunoreactivity (total area of pixels above the threshold) (average of one slice from three mice per group). The mean intensity of the entire image was measured in each section. (c–e) Immunohistochemical images showing colocalization of the endothelial cell marker tomato lectin or the astrocyte marker Aldh1l1 and AGEs. (f, g) Plots of pixel intensities along the white arrow in d and e, respectively. The black arrows in f indicate colocalization points of lectin and AGEs. (h) Immunohistological images of GFP-positive astrocytes in the hippocampal CA1 region. (i) Number of GFP-positive cells in each image presented in h. No significant differences were observed among the groups. (k) Mean fluorescent intensities of 10 randomly selected cells per image from the hippocampal CA1 region (from four independent mice). Tukey–Kramer tests were used in b, i, and j. $^{**}P < 0.01$; $^{***}P < 0.001$.

Fig. 4 Angiopathy and impaired glucose transport in G × E mice.

(a, b) Venn graph showing the overlap in prefrontal cortex genes exhibiting a >2-fold (a) or <0.5-fold (b) expression change compared with the CTL group (n = 3 mice per group). (c) Immunohistochemical images of fibrin and the endothelial cell marker tomato lectin. (d) Measurement of the area covered by fibrin immunoexpression in c (defined as the area of pixels above threshold of pixel intensity in each image) (average of one slice from three mice per group). The mean intensity of the entire image was measured for each section. (e) Immunohistochemical images of fibrin and tomato lectin in medial prefrontal cortex. (f) Plots of pixel intensities along the yellow arrow in e. (g) Extracellular concentrations of glucose in the dialysis buffer at each time point (1 h collection after 16 h of fasting, 0–1 h after eating 0.05 g of carbohydrate (starch or sucrose), and 1–2 h after eating 0.05 g of carbohydrate (starch or sucrose) (n = 5–6 mice per group)). (h) Plasma glucose levels in wild-type (WT) and *Glo1* heterozygous mice (n = 6–7 mice per group). The first measurement was performed after 16 h of fasting, and the second blood collection was performed 30 min after eating 0.05 g of carbohydrate. No significant differences were observed among groups. (i) Fasting plasma insulin levels in WT and *Glo1* heterozygous mice. No significant differences were observed between groups (n = 5–6 mice per group). Two-way repeated-measures ANOVA was used in g and h. Main effects of group were as follows:

g ($F_{3, 23} = 5.7851$, $P = 0.0042$) and h ($F_{3, 23} = 2.9734$, $P = 0.0528$). Tukey–Kramer tests were used in d and i. The data are presented as the mean ± s.e.m. $^{**}P < 0.01$; $^{*}P < 0.05$.

Fig. 5 Protective effects of low-dose aspirin in G × E mice.

(a–d) Results of behavioral tests performed to evaluate the effects of aspirin treatment (n = 12–21 mice per group). (a) Quantifications of spontaneous locomotor activity in the open field. (b) Pre-pulse inhibition at 70 dB. (c) Object location test of working memory. (d) Quantification of nest building skills over 8 h (n = 12–21 mice per group). (e) Immunohistochemical images of fibrin and the endothelial cell marker tomato lectin. (f) Measurement of the area covered by fibrin immunoexpression in e (defined as the area of pixels above the threshold of pixel intensity in each image) (average of one slice from three mice per group). The mean intensity of the entire image was measured for each section. (g) Extracellular concentrations of glucose in the dialysis buffer at each time point (1 h collection after 16 h of fasting, 0–1 h after eating 0.05 g of carbohydrate, and 1–2 h after eating 0.05 g of carbohydrate) (n = 4–6 mice per group). Tukey–Kramer tests were used in b, c, and f, two-way repeated-measures ANOVA in a and d. The main effects of group were as follows: a ($F_{2, 50} = 6.4385$, $P = 0.0033$), d ($F_{2, 49} = 8.0315$, $P = 0.001$), and g ($F_{2,}$

17 = 6.1758, $P = 0.0096$). The data are presented as the mean ± s.e.m. *$P < 0.05$; **$P < 0.01$; ***$P < 0.01$.

Fig. 6 Angiopathy in postmortem brains from individuals with psychiatric disorders. (a) Representative immunohistochemical images of fibrin in the BA9 region of postmortem brains from controls and patients with schizophrenia (SZ) or bipolar disorder (BD). (b) Measurement of the area covered by fibrin immunoexpression in a (defined as area of pixels above threshold of pixel intensity in each image. The mean intensity of the entire image was measured for each section. The Tukey–Kramer test was used in b. Data are presented as the mean ± s.e.m. (c) Representative immunohistochemical images of fibrin (magenta) and the endothelial cell marker tomato lectin (green) in postmortem brains from a SZ patient. Fibrin-positive areas are merged with areas of vascular endothelial cell marker expression. (d) Diagrams describing the hypothesis proposed to explain functional and behavioral abnormalities in CTL mice (left) and G × E mice (right) (see Discussion for details).

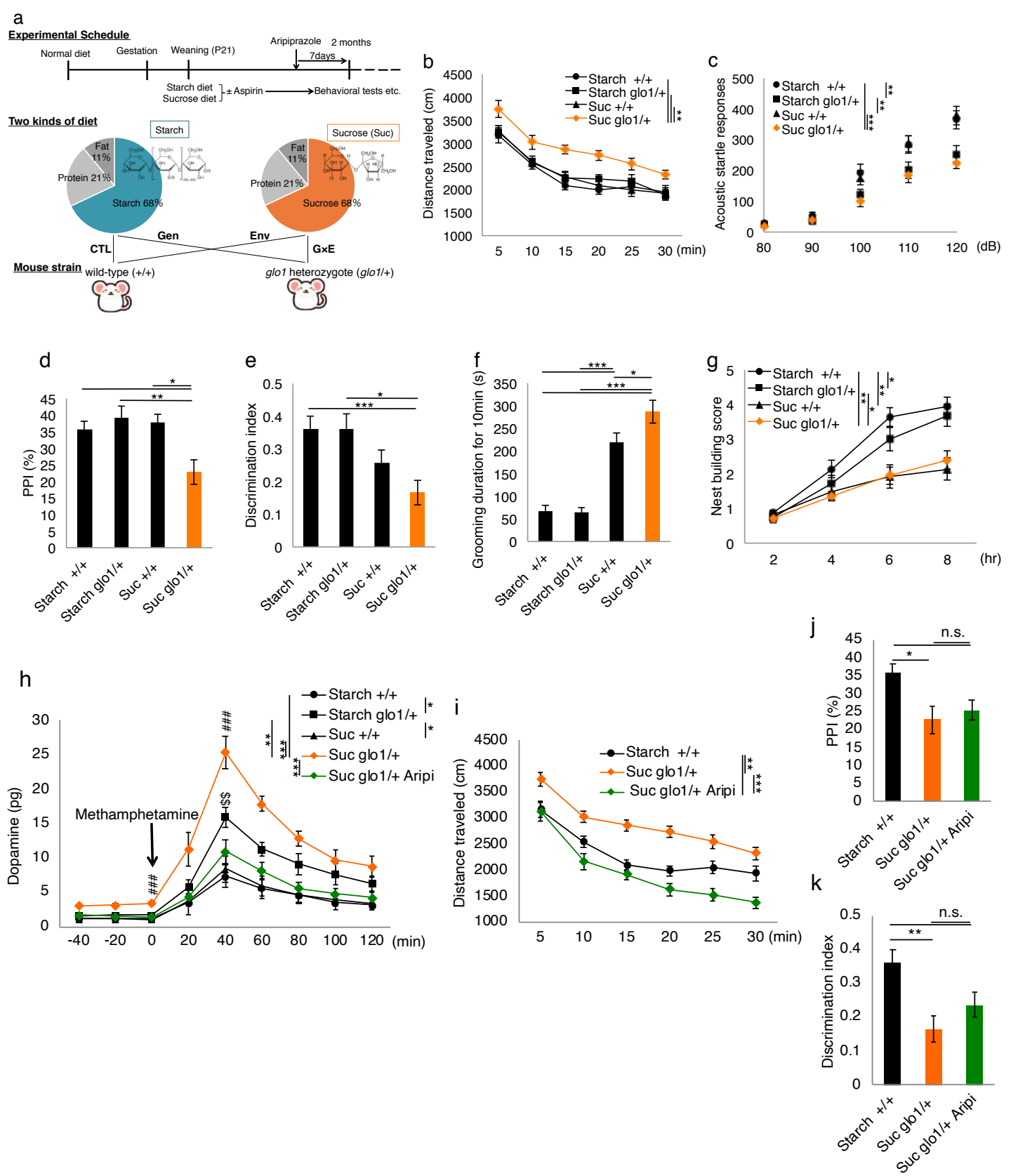
a
Experimental Schedule
Normal diet
Gestation
Weaning (P21)
Aripiprazole
2 months
7days
Starch diet
Sucrose diet
± Aspirin
Behavioral tests etc.
Two kinds of diet
Starch
Fat 11%
Protein 21%
Starch 68%
Sucrose (Suc)
Sucrose 68%
Gen
Env
CTL
G×E
Mouse strain
wild-type (+/+)
glo1 heterozygote (glo1/+)
b
Distance traveled (cm)
Starch +/+
Starch glo1/+
Suc +/+
Suc glo1/+
(min)
c
Acoustic startle responses
(dB)
d
PPI (%)
e
Discrimination index
f
Grooming duration for 10min (s)
g
Nest building score
(hr)
h
Dopamine (pg)
Methamphetamine
Starch +/+
Starch glo1/+
Suc +/+
Suc glo1/+
Suc glo1/+ Aripi
(min)
i
Distance traveled (cm)
Starch +/+
Suc glo1/+
Suc glo1/+ Aripi
(min)
j
PPI (%)
n.s.
Starch +/+
Suc glo1/+
Suc glo1/+ Aripi
k
Discrimination index
n.s.
Starch +/+
Suc glo1/+
Suc glo1/+ Aripi

Figure 1

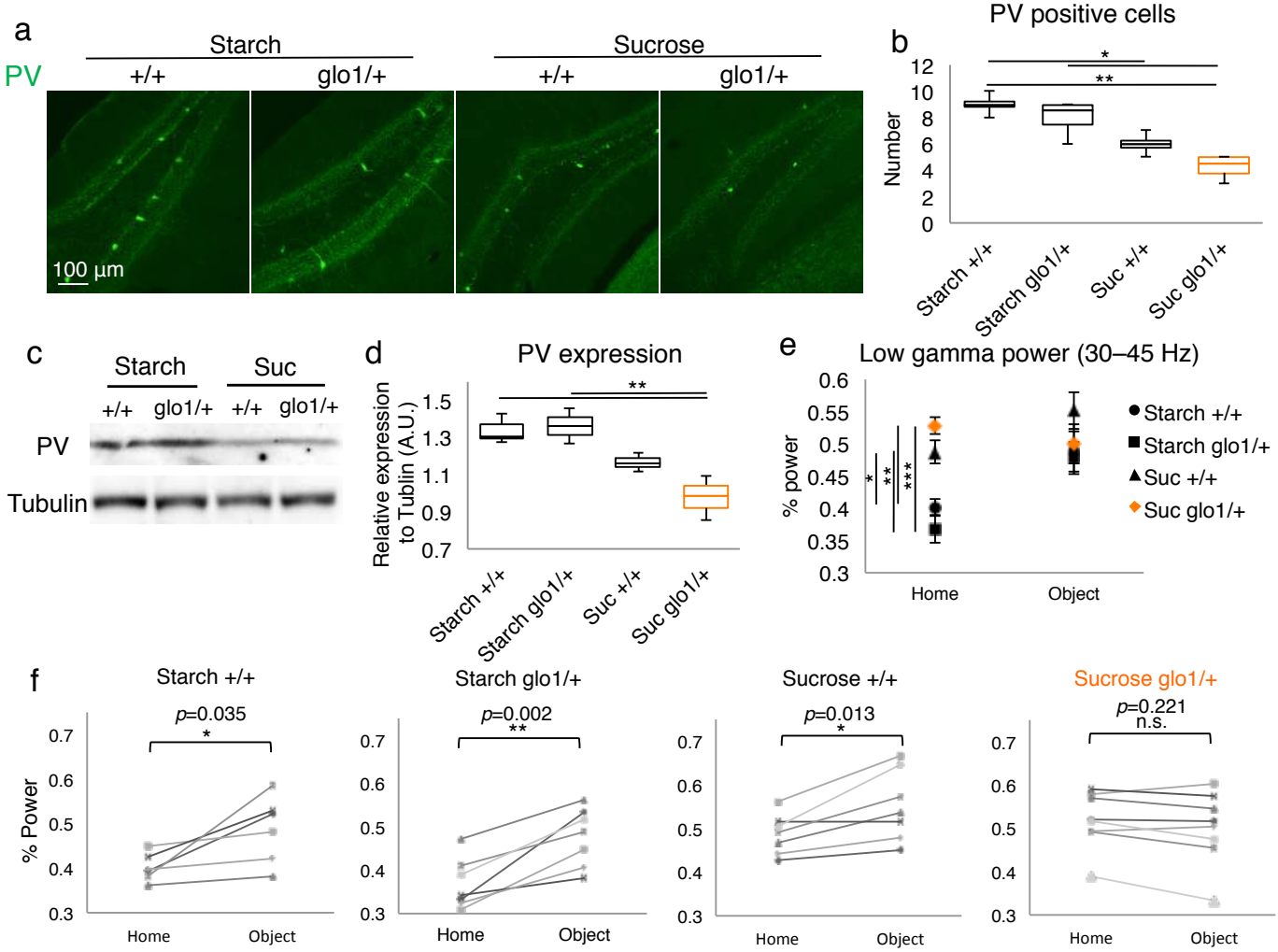
a
Starch
Sucrose
PV
+/+
glo1/+
+/+
glo1/+
100 µm
b
PV positive cells
Number
Starch +/+
Starch glo1/+
Suc +/+
Suc glo1/+
c
Starch
Suc
+/+
glo1/+
+/+
glo1/+
PV
Tubulin
d
PV expression
Relative expression to Tublin (A.U.)
e
Low gamma power (30–45 Hz)
% power
Home
Object
f
Starch +/+
p=0.035
Starch glo1/+
p=0.002
Sucrose +/+
p=0.013
Sucrose glo1/+
p=0.221
n.s.
% Power
Home
Object

Figure 2

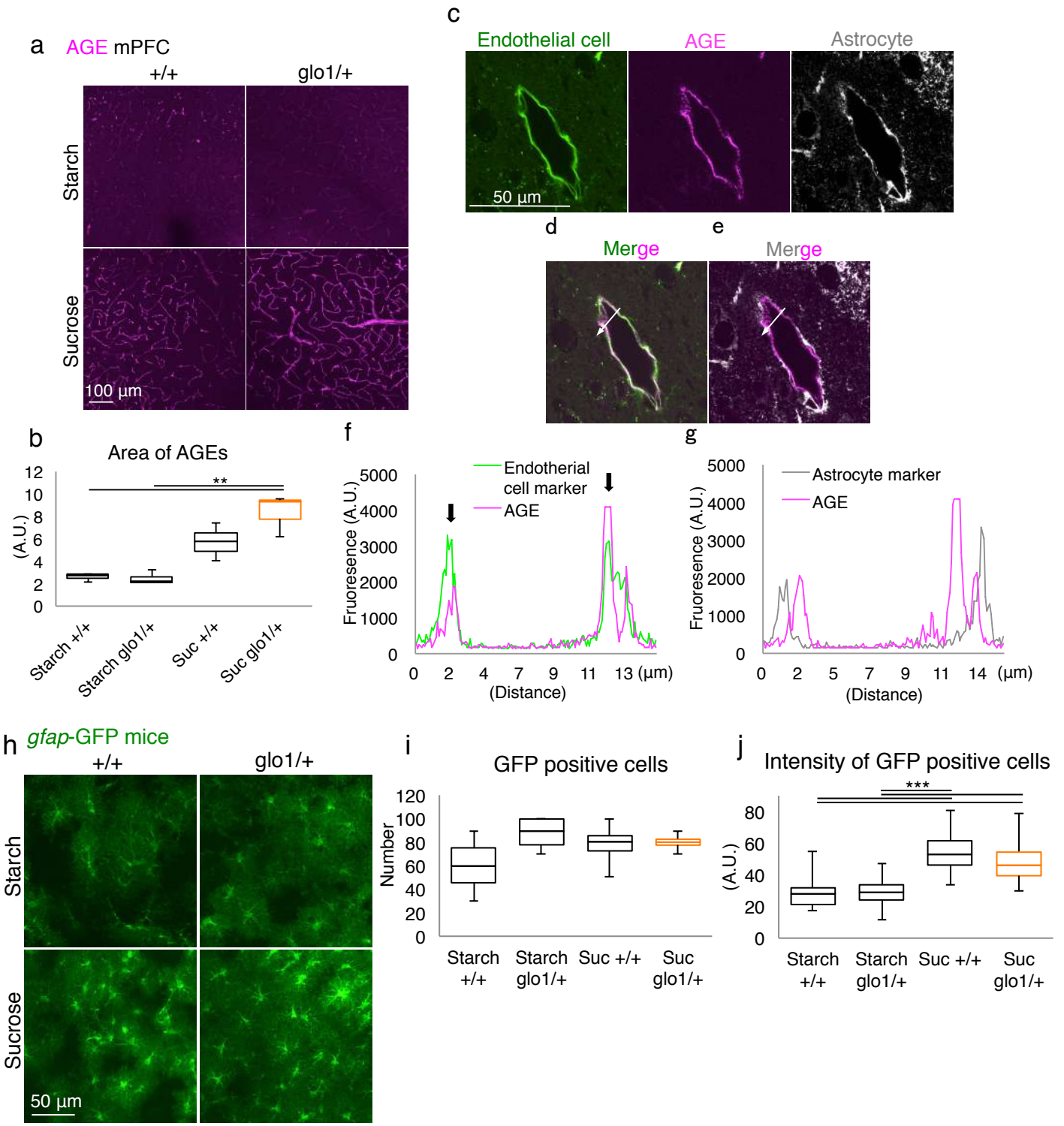
a
AGE mPFC
+/+
glo1/+
Starch
Sucrose
100 µm
b
Area of AGEs
(A.U.)
**
Starch +/+
Starch glo1/+
Suc +/+
Suc glo1/+
c
Endothelial cell
AGE
Astrocyte
50 µm
d
Merge
e
Merge
f
Endotherial cell marker
AGE
Fluoresence (A.U.)
(Distance)
g
Astrocyte marker
AGE
Fluoresence (A.U.)
(Distance)
h
gfap-GFP mice
+/+
glo1/+
Starch
Sucrose
50 µm
i
GFP positive cells
Number
Starch +/+
Starch glo1/+
Suc +/+
Suc glo1/+
j
Intensity of GFP positive cells
***
(A.U.)
Starch +/+
Starch glo1/+
Suc +/+
Suc glo1/+

Figure 3

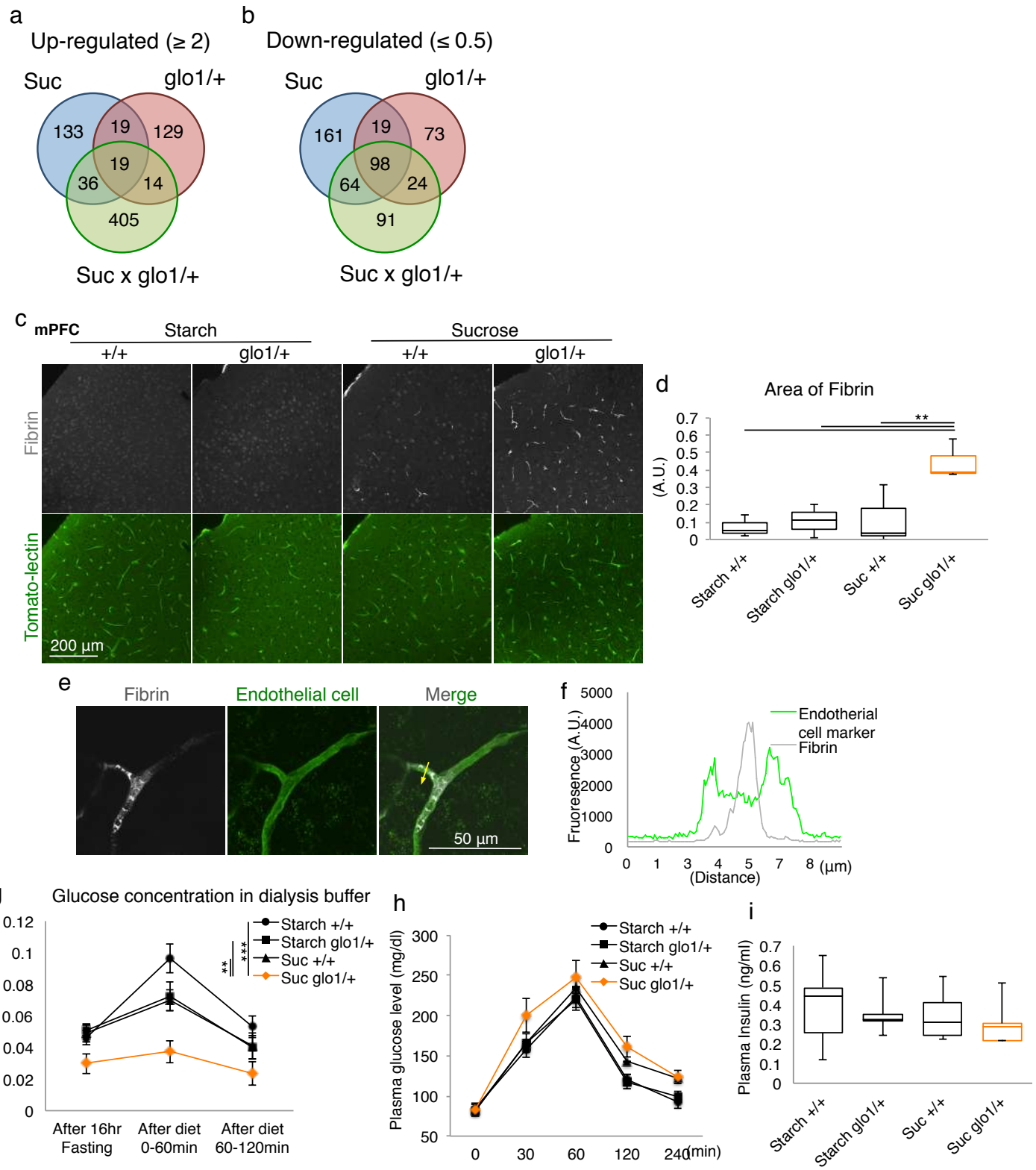
a
Up-regulated (≥ 2)
Suc
glo1/+
133
19
129
19
36
14
405
Suc x glo1/+
b
Down-regulated (≤ 0.5)
Suc
glo1/+
161
19
73
98
64
24
91
Suc x glo1/+
c
mPFC
Starch
Sucrose
+/+
glo1/+
+/+
glo1/+
Fibrin
Tomato-lectin
200 μm
d
Area of Fibrin
(A.U.)
0.7
0.6
0.5
0.4
0.3
0.2
0.1
0
**
Starch +/+
Starch glo1/+
Suc +/+
Suc glo1/+
e
Fibrin
Endothelial cell
Merge
50 μm
f
Fluoresence (A.U.)
5000
4000
3000
2000
1000
0
Endotherial cell marker
Fibrin
0 1 3 4 5 7 8 (μm)
(Distance)
g
Glucose concentration in dialysis buffer
Glucose (mM)
0.12
0.1
0.08
0.06
0.04
0.02
0
**
***
Starch +/+
Starch glo1/+
Suc +/+
Suc glo1/+
After 16hr Fasting
After diet 0-60min
After diet 60-120min
h
Plasma glucose level (mg/dl)
300
250
200
150
100
50
Starch +/+
Starch glo1/+
Suc +/+
Suc glo1/+
0
30
60
120
240
(min)
i
Plasma Insulin (ng/ml)
0.7
0.6
0.5
0.4
0.3
0.2
0.1
0
Starch +/+
Starch glo1/+
Suc +/+
Suc glo1/+

Figure 4

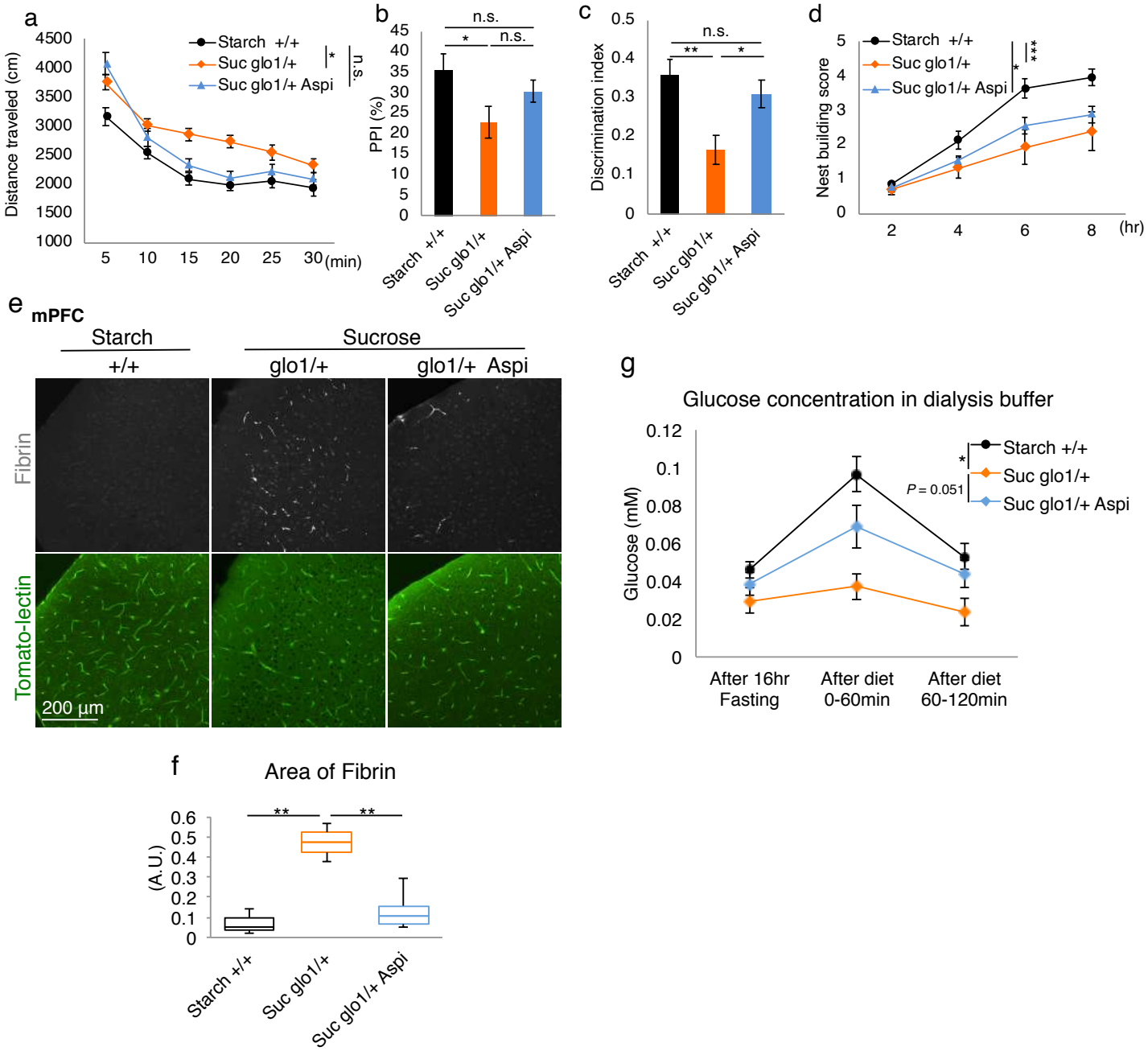
a
Distance traveled (cm)
Starch +/+
Suc glo1/+
Suc glo1/+ Aspi
*
n.s.
(min)
b
PPI (%)
n.s.
*
n.s.
Starch +/+
Suc glo1/+
Suc glo1/+ Aspi
c
Discrimination index
n.s.
**
*
Starch +/+
Suc glo1/+
Suc glo1/+ Aspi
d
Nest building score
Starch +/+
Suc glo1/+
Suc glo1/+ Aspi
*
***
(hr)
e
mPFC
Starch
Sucrose
+/+
glo1/+
glo1/+ Aspi
Fibrin
Tomato-lectin
200 µm
f
Area of Fibrin
(A.U.)
**
**
Starch +/+
Suc glo1/+
Suc glo1/+ Aspi
g
Glucose concentration in dialysis buffer
Glucose (mM)
Starch +/+
Suc glo1/+
Suc glo1/+ Aspi
*
P = 0.051
After 16hr Fasting
After diet 0-60min
After diet 60-120min

Figure5

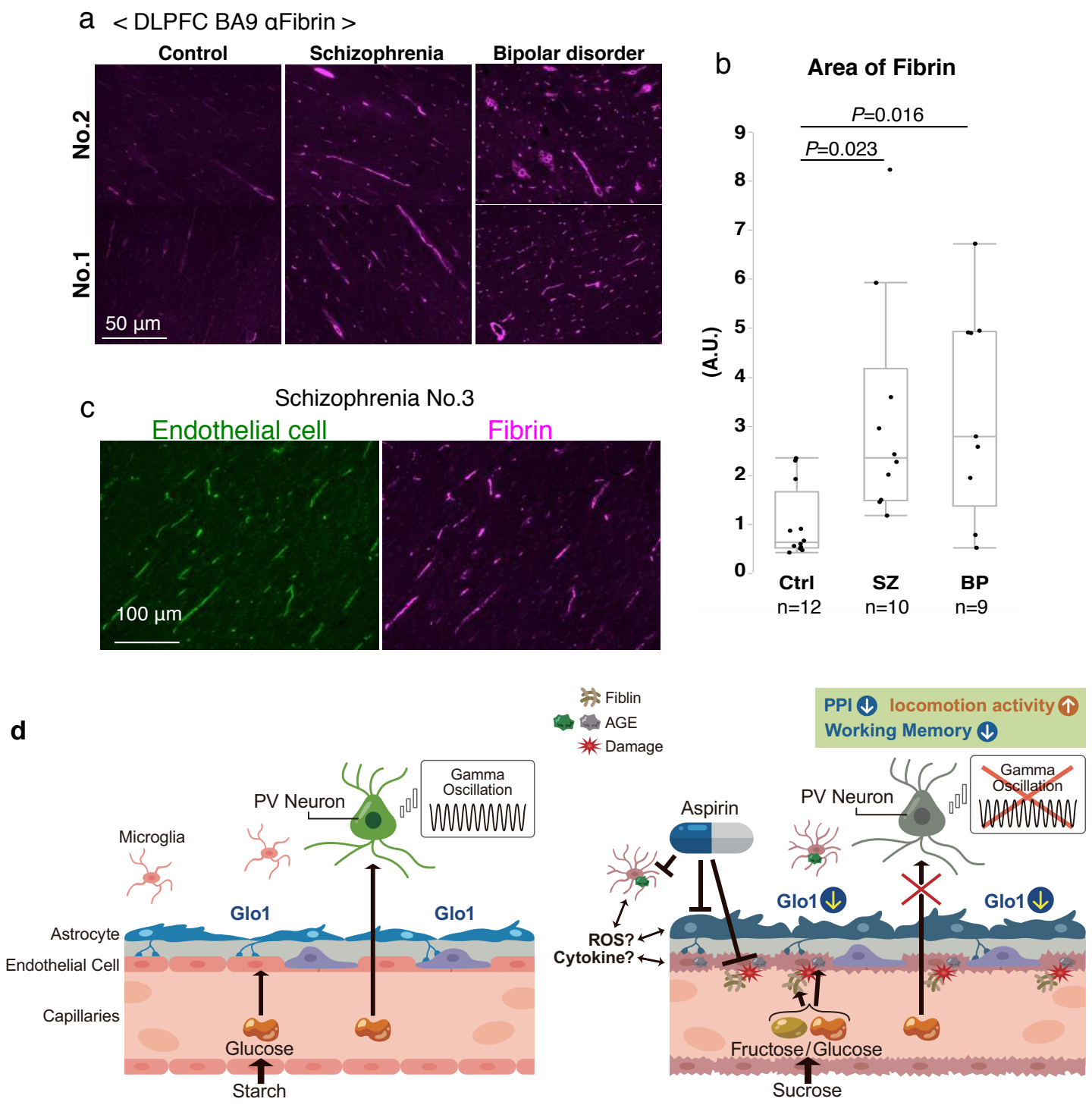
a
< DLPFC BA9 αFibrin >
Control
Schizophrenia
Bipolar disorder
No.2
No.1
50 μm
b
Area of Fibrin
P=0.016
P=0.023
(A.U.)
0
1
2
3
4
5
6
7
8
9
Ctrl
n=12
SZ
n=10
BP
n=9
c
Schizophrenia No.3
Endothelial cell
Fibrin
100 μm
d
Fiblin
AGE
Damage
PPI
locomotion activity
Working Memory
PV Neuron
Gamma Oscillation
Microglia
Glo1
Glo1
Astrocyte
Endothelial Cell
Capillaries
Glucose
Starch
Aspirin
ROS?
Cytokine?
Glo1
Glo1
Fructose/Glucose
Sucrose

Figure 6